

How Complex is the Magmatic System Beneath Sakurajima Volcano and Aira Caldera?

Submitted by Robert Backhurst to the University of Exeter
as a thesis for the degree of
Masters by Research in Geology
In January 2022

Supervisors: James Hickey & Ben Williamson

This thesis is available for Library use on the understanding that it is copyright material and that no quotation from the thesis may be published without proper acknowledgement.

I certify that all material in this thesis which is not my own work has been identified and that no material has previously been submitted and approved for the award of a degree by this or any other University.

Signature: 

Abstract

Our understanding of the subsurface processes that cause volcanic unrest is currently incomplete, impacting our ability to predict eruptive episodes and protect communities at risk from volcanic hazards. Monitoring and modelling of ground deformation has become one of the main methods for evaluating the potential for volcanic unrest, however basic modelling techniques usually require too many assumptions to be realistic. In this thesis, volcano deformation has been assessed and modelled using Finite Element Analysis (FEA), to increase the accuracy of identifying the origins of observable surface deformation. Simplified modelling of a vertically stacked, double reservoir magmatic system showed that major magmatic reservoirs can dominate surface displacement fields during deformation episodes. Displacement contributions from shallower, smaller storage regions can be obscured from modern geodetic monitoring equipment, hiding their presence within the magmatic system, and impacting eruption forecasts and hazard assessments. Understanding how individual parameters behave in a 2D environment set a benchmark for more realistic 3D modelling. This framework was then applied to assess Aira caldera in Japan, to re-examine a period of deformation around the caldera and Sakurajima volcano utilizing FEA, assuming a multiple pressure source magmatic system. With the inclusion of topography and subsurface heterogeneities, modelling identified a shallow magmatic reservoir that may account for uncertainties in earlier models, which assumed a single magmatic source. Additional models analysed Bouguer gravity data to scrutinize shallow reservoir parameters, which highlighted the potential of combining deformation and gravity modelling approaches to produce higher accuracy magmatic storage estimates for Aira caldera, as well as other volcanic systems worldwide. Uncertainties remain in fully representing crustal characteristics, which will continue to restrict the potential of future geodetic modelling. However, the FEA work presented in this thesis gives a framework for improved interpretation of deformation events.

Acknowledgments

Firstly, I must thank my main supervisor, James. Your assistance and patience with me throughout this Masters process has been invaluable, from helping grasp a few of the complexities of COMSOL, to giving me the opportunity to undertake this project at all in an amazing part of the country. To my secondary supervisor, Ben, thank you for your help and guidance, especially in the final production of this thesis.

This journey is only reaching its conclusion thanks to my friends, both new and old, and my family, who have all encouraged and motivated me throughout these past two years. I am indebted to you all.

Lastly, to Mum, Dad, and Victoria, thank you for your love and support, and for inspiring me to go for challenges beyond my comfort zone.



*Master's student Rob,
Attempts to use computers,
In lots of pages.*

Contents

Abstract.....	2
Acknowledgments.....	3
Contents.....	5
List of Figures.....	7
List of Tables	8
Chapter 1: Introduction.....	9
1.1 Background and Motivation.....	10
1.2 Thesis Aims.....	12
1.3 Thesis Structure	12
Chapter 2: Volcano Geodesy and the Volcanism of Aira Caldera, Japan	14
2.1 Introduction.....	15
2.2. Volcano Geodesy and Modelling	15
2.2.1 Volcano Deformation.....	15
2.2.2 Deformation Modelling	17
2.2.3 Gravity Modelling	20
2.3. The Geology and Volcanism of Japan	22
2.3.1 The Geography and Geological History of Japan	22
2.3.2 The History of Kyushu and Sakurajima.....	24
2.3.3 Sakurajima Volcano Monitoring and Modelling History	26
Chapter 3: Shallow Pressure Source Contributions to Surface Displacement Patterns in a Stacked Magma Reservoir Setup.....	31
3.1 Introduction.....	32
3.2 Methods.....	33
3.2.1 Model Setup	33
3.2.2 Modelling Approach	35
3.3 Results	37
3.3.1 Depth.....	37
3.3.2 Volume	38
3.3.3 Overpressure	38
3.4 Discussion	39
3.4.1 Source Shape	39
3.4.2 Direction Component	40
3.4.3 Implications	41
3.5 Limitations	42
3.6 Conclusions.....	43
Chapter 4: Multiple Pressure Source Numerical Deformation Modelling of the Sakurajima Volcano and Aira Caldera Magmatic System.....	45

4.1 Introduction.....	46
4.2 Methods.....	50
4.2.1 Datasets	50
4.2.2 Deformation Model Setup	52
4.2.3 Deformation Modelling Approach.....	54
4.2.4 Gravity Modelling	56
4.3 Results	58
4.3.1 Shallow Pressure Sources.....	58
4.3.2 Bouguer Anomaly Distributions.....	61
4.4 Discussion	62
4.4.1 Shallow Source Location	62
4.4.2 Shallow Source Overpressure	65
4.4.3 Applicability of Gravity Modelling Approach.....	65
4.4.4 Other Limitations	66
4.5 Conclusions.....	67
Chapter 5: Concluding Remarks.....	69
5.1 Thesis Summary	70
5.2 Implications and Limitations	72
5.2.1 Crustal Rheology.....	72
5.2.2 Combined Deformation and Gravity Modelling	73
5.2.3 Multiple Pressure Source Modelling	74
5.3 Future Applications.....	75
References	77

List of Figures

2.1: ‘Mogi’ model arrangement.....	19
2.2: Example FEM setup	20
2.3: Tectonic map of Japan	23
2.4: Volcanic Region map of Kyushu	25
2.5: Kagoshima Bay and Sakurajima volcano locations	27
2.6: Deformation history of Aira caldera	28
3.1: Double pressure source FEM arrangement.	34
3.2: Basic modelled subsurface heterogeneity	35
3.3: Uplift difference values when varying depth	38
3.4: Uplift difference values when varying volume	39
3.5: Uplift difference values when varying overpressure	40
3.6: Maximum modelled displacements	41
4.1: The geography of Kagoshima Bay	48
4.2: Deformation and recent eruptive history of Sakurajima.....	49
4.3: Measured GPS deformation at Aira caldera from 1996 – 2007.....	51
4.4: Measured Bouguer anomaly distribution across Kagoshima Bay	52
4.5: Finite element model for Aira caldera.....	53
4.6: Grid coordinates.....	55
4.7: Source shape parameter sensitivity test misfit values	59
4.8: Frequency of best fit parameters.....	60
4.9: Modelled best fit deformation vectors.....	61
4.10: Gravity modelling misfits.....	62
4.11: Modelled Bouguer anomalies and misfits	63

List of Tables

3.1: Full range of shallow source parameters tested	36
3.2: Tested range of shallow source shape, volumes, and axes lengths	37
4.1: Previous best fit pressure source solutions	50
4.2: Full range of shallow source parameters tested.....	55
4.3: Tested range of source shapes and sizes.....	55
4.4: Top 10 grid search parameter arrangements.....	60

Chapter 1: Introduction

1.1 Background and Motivation

Over the last 10,000 years, around 1,500 terrestrial volcanoes have shown some form of activity [LaFemina, 2015]. Today, across 86 countries, an estimated 800 million people reside within a 100 km radius of an active volcano [Acocella, 2021]. Countries such as Japan, Indonesia, and Mexico are at particular risk due to the proximity of densely populated areas to volcanic centers [UNISDR, 2015]. A significant threat to life is ever-present in these regions, with eruptions capable of claiming thousands of lives. The 1985 Nevado del Ruiz eruption in Colombia, for example, caused around 23,000 fatalities [Pierson *et al.*, 1990]. Volcanic eruptions can also threaten infrastructure; the 2010 Eyjafjallajökull eruption in Iceland resulted in zero deaths, but caused around US \$5 billion damage [Acocella, 2021]. The vital importance of being able to better forecast eruptive activity drives research into volcanism around the world. Despite all of the rapid scientific advances in volcano monitoring, accurate forecasting is not always attainable [Sparks *et al.*, 2012], as a full understanding of volcano dynamics and signatures related to precursory activity is lacking [Desai *et al.*, 2015].

Volcanic unrest is defined as a period when activity levels exceed the base levels of the volcano in question, and are a cause for concern. [Phillipson *et al.*, 2013]. Episodes of unrest may result in volcanic events, presenting a danger to surrounding population centers. Successful forecasting to mitigate risks of potential volcanic events requires an understanding of monitoring signals from the volcano, as well as the location and nature of unrest, meaning detailed knowledge of the processes within the subsurface of a volcanic system is crucial. One of the main manifestations of volcanic unrest is surface deformation, where the magnitudes and orientations of inflation or deflation may signal the build-up to volcanic events [Sparks *et al.*, 2012; Phillipson *et al.*, 2013; Biggs *et al.*, 2014, 2017; Fernández *et al.*, 2017; Hickey *et al.*, 2017]. Surface deformation patterns, in space and time, can be used to locate and constrain the origins of deformation within the crust [Dvorak *et al.*, 1997; Dzurisin, 2003, 2007; Poland *et al.*, 2006], typically via geodetic modelling. Traditionally, modelling efforts have been relatively simple, due to limitations in understanding and computer processing powers. In the traditional analytical models, the Earth's crust is assumed to be a homogeneous, elastic, isotropic, half space with no topography, and the causes of deformation are simulated assuming pressure point sources [Mogi, 1958], or

as finite spheroidal cavities [McTigue, 1987; Yang *et al.*, 1988; Fialko *et al.*, 2001]. Whilst useful for initial assessments in eruption forecasting and hazard assessment, the assumptions required for analytical techniques limit the accuracy of the models, for example failing to incorporate heterogenous crustal conditions, and therefore potentially misrepresenting the processes occurring within magmatic systems [Currenti *et al.*, 2007; Masterlark, 2007; Hickey *et al.*, 2013, 2016].

Overcoming the limitations of analytical models can be achieved by using more advanced numerical methods [Jing *et al.*, 2002]. The use of the Finite Element Method, a technique increasingly employed in the field of volcano geodesy [Dieterich *et al.*, 1975], is growing in popularity as computational capabilities, precision of geological and geophysical data, and our understanding of rock mechanics have all increased [Zienkiewicz *et al.*, 2000; Gottsmann *et al.*, 2006; Currenti *et al.*, 2007, 2008; Grosfils, 2007; Masterlark, 2007; Del Negro *et al.*, 2009; Gregg *et al.*, 2012, 2013; Hickey *et al.*, 2013; Gottsmann, Biggs, *et al.*, 2020]. One of the main benefits of modelling using Finite Element analysis is the inclusion of a heterogenous subsurface mechanical structure, consisting of rock layers of varying densities and stiffnesses, which is more realistic for volcanic regions [Gudmundsson, 2006, 2012]. Crucially, stress fields vary spatially in heterogenous domains when an overpressure is applied to the magmatic system, with models subsequently displaying surface deformation patterns that are different to equivalent models constructed in homogenous domains [Geyer *et al.*, 2010; Hautmann *et al.*, 2010]. Analysis of deformation patterns using models with heterogeneous subsurface structures can have different source locations and strengths compared with those produced by analytical methods [Currenti *et al.*, 2007; Masterlark, 2007; Hickey *et al.*, 2016]. To observe the differences in numerical and analytical approaches, it is optimal to study a volcano with an extensive analytical deformation modelling history, but that also possesses the necessary data to apply numerical techniques.

Aira caldera, in southern Kyushu, Japan, is an ideal case example on which to apply modern numerical modelling techniques. Little variance has been applied in past modelling studies, which has an emphasis on analytical methods. The caldera remains active today and is constantly monitored, with an active GPS network surrounding the caldera to observe ground deformation, providing a

wealth of geodetic data. The modelling of multiple pressure sources within the Aira caldera magmatic system, using modern numerical techniques, and increased computing capacity, has not been attempted. This gap in knowledge presents an opportunity to conduct extensive numerical modelling of the Aira caldera magmatic system, to yield results which could be directly compared with analytical results from equivalent time periods. An enhanced understanding of the origins of surface deformation from subsurface processes at Aira caldera could aid future forecasting of eruptive events of the volcano, and from volcanoes worldwide.

1.2 Thesis Aims

To date, no deformation models have been conducted at Aira caldera to test for the presence of multiple magmatic sources using numerical methods, nor have any been attempted utilizing both deformation and gravity data. This thesis will model multiple pressure sources within a magmatic system with the following aims:

- Assess the impact of changes in depth, overpressure, and geometry of secondary shallow pressure sources on the resulting displacement profiles of single and double source magmatic systems, using Finite Element models.
- Determine a best fit arrangement for the Aira caldera magmatic system, and explore optimal parameters for any potential shallow sources within the system.
- Test the effectiveness of comparing gravity anomalies resulting from different magmatic source arrangements within the Aira caldera magmatic system, to scrutinize potential best fit arrangements from the deformation modelling process.

1.3 Thesis Structure

This thesis consists of an introduction chapter, followed by a literature review, a 2D numerical modelling study, the main research at Aira caldera, and a conclusions chapter. The chapter on Aira caldera is in preparation for a journal submission, and is presented like a published paper for consistency.

Chapter 2 is a review of the literature on the scope of volcano deformation, its main modelling techniques and limitations, and the methods used for later chapters of this thesis. It also contains a description of the geology and volcanic history of Japan, in particular Sakurajima volcano.

Chapter 3 focuses on the modelling of surface deformation patterns in a 2D axisymmetric model. Comparisons and analyses between deformation patterns of vertically stacked single and double magmatic source systems, highlight the sensitivity of surface data to different depths, overpressures, and sizes of shallow pressure sources, to inform parameter tests in models presented in Chapter 4.

Using the foundations gained in Chapter 3, Chapter 4 applies similar methods in a 3D model of Aira caldera and Sakurajima volcano in Japan. Using full subsurface heterogeneity provided by seismic tomography of the volcanic regions, Finite Element modelling is used to simulate deformation patterns, and test the hypothesis that multiple pressure sources are present within the magmatic system. Subsurface density variations are also used to model Bouguer gravity fields, to assist in defining best fit parameters of any shallow secondary source inferred in the magmatic system. The best fit model results are discussed and compared to equivalent outcomes from past modelling, and considerations given to their implications for future studies.

Lastly, Chapter 5 reviews the results from the previous chapters, identifies improvements which could be made in future modelling, and discusses the global significance for numerical modelling of volcano deformation.

Chapter 2:
Volcano Geodesy and the Volcanism
of Aira Caldera, Japan

2.1 Introduction

Volcanic unrest is defined as “*a period of elevated activity of a particular volcano compared to the normal background levels, causing concern for a potential eruption*” [Phillipson *et al.*, 2013]. Monitoring volcanic unrest is of vital importance to aid forecasting of eruptions, hazard assessment, and risk mitigation. Volcanic activity manifests at the surface but originates at depth, and therefore understanding the subsurface processes that could lead to an eruption are crucial. The methods for monitoring volcanic unrest are derived from three related fields: geochemistry, seismology, and geodesy; and are most accurate if these are combined. An important aspect to volcanic unrest monitoring is understanding the magmatic “plumbing” system of a volcano, which can at least be partly achieved through observing and interpreting volcanic deformation [Sparks *et al.*, 2012; Phillipson *et al.*, 2013; Biggs *et al.*, 2014, 2017; Fernández *et al.*, 2017]. Ground deformation can imply changing subsurface magmatic conditions, as magma migrates laterally or vertically [Dvorak *et al.*, 1997; Dzurisin, 2003, 2007; Poland *et al.*, 2006], or non-magmatic processes such as hydrothermal activity [e.g., Kereszturi *et al.*, 2021]. Surface displacements can be assessed and monitored using a wide variety of instruments, producing data which can be interpreted in near real-time, and then used in subsequent models. This chapter discusses volcano deformation in detail, historical and current modelling techniques that utilise deformation data, and introduces the well-documented Sakurajima volcano in Japan, which has a detailed history of inflation and deflation periods ideal for analysis through deformation modelling.

2.2. Volcano Geodesy and Modelling

2.2.1 Volcano Deformation

The field of volcanic geodesy focuses on how surface deformation changes in space and time as a result of volcanic processes [Dzurisin, 2003, 2007]. Surface deformation can manifest as inflation episodes resulting from subsurface magma accumulation [Parks *et al.*, 2012] or subsidence associated with withdrawal or cooling of magma at depth [Gudmundsson *et al.*, 2016]. However, it can also be the result of a variety of non-magmatic mechanisms, for example changes in related hydrothermal systems [Kereszturi *et al.*, 2021], cooling of previously emplaced magmas [Hamling *et al.*, 2015], volcanic edifice instabilities

[*Bonaccorso et al.*, 2013], or deposit loading [*Odbert et al.*, 2015]. The complexity of determining the exact cause of ground displacements are one of the main uncertainties in eruption forecasting and hazard assessment [*Cashman et al.*, 2013; *Sparks et al.*, 2017].

Modern geodetic monitoring networks, available at numerous volcanoes worldwide, are sophisticated in combining a wide variety of ground instrumentation and satellite arrays, providing precise and continuous or near-continuous observations [*Dzurisin*, 2007; *Sparks et al.*, 2012; *Biggs et al.*, 2014, 2017; *Pinel et al.*, 2014]. A simple way to observe deformation is manual measurement of relative ground heights using a method called levelling. Levelling surveys are field campaigns that measure the observed height of benchmarked reference points from distinct locations within a network [*Dzurisin*, 2007]. Conducting repeat surveys at the same locations allows for the relative change in height of these reference points to be measured through time [*Dzurisin et al.*, 1991, 2002].

Tiltmeters are also used to assess changes in surface angle or inclination. When magma accumulates beneath a volcano, the surface above can tilt away from the centre of uplift as the surface bulges, with the inverse occurring as magma drains from a reservoir [*Dzurisin*, 1992]. A network of tiltmeters around a volcanic edifice can be used to measure this change in angle and inform on the scale and depth of magmatic intrusions [*Wicks et al.*, 2001, 2002a, 2002b]. Whilst giving precise data, measuring deformation using discrete, time-separated campaign surveys has considerable disadvantages. It is slow, and can only output data during survey campaigns, making it unsuitable for monitoring of active volcanoes where better temporal resolutions are required. A network of permanent instruments is usually much more effective as it can give continuous results in real time [*Acocella*, 2021].

Satellite monitoring techniques are widely used to monitor surface displacements, with the most common being Interferometric Synthetic Aperture Radar (InSAR) and Global Positioning Systems (GPS). InSAR enables monitoring of ground deformation over 10's of kilometres with cm scale precision, and is achieved by combining radar images from similar angles over the same area from different time periods [*Massonnet et al.*, 1993, 1998; *Bürgmann et al.*,

2000]. Despite only outputting measurements when the satellite has line-of-sight of the study area, and after multiple passes have been conducted (e.g., every 6 – 12 days for the European Space Agency's Sentinel-1 [Geudtner *et al.*, 2014]), radar based monitoring techniques such as InSAR can operate in most weather conditions, making it especially useful during volcanic events and in remote locations [Sparks *et al.*, 2012].

GPS uses a series of receivers, typically installed as a network surrounding a volcano, transmitting location data to orbiting satellites [Leick, 1990; Iguchi *et al.*, 2008]. GPS receivers can determine displacements along three different axes, with accuracies of a few millimetres for N-S and E-W horizontal components, and around 10 mm for the vertical component [Dzurisin, 2007; Acocella, 2021]. Measurements are collected through permanent, autonomous stations, or through campaign style surveys at varying frequencies. Permanent networks can output high resolution, continuous data, but only at certain locations where the receivers are installed. Campaign surveys do have the flexibility to be conducted anywhere, but at the cost of losing real-time effectiveness. Balancing sampling rate and data accuracy is a challenge for any volcano monitoring network and can be expensive; cost is often the deciding factor between what monitoring data collection methods are included in a network [Dzurisin, 2003; Acocella, 2021].

Techniques such as InSAR, levelling, and continuous GPS networks, provide an abundance of positional data in the monitoring of unrest. However, understanding the exact processes driving measured deformation in any magmatic system requires a further level of analysis through modelling.

2.2.2 Deformation Modelling

Geodetic data can be used to infer the source of deformation by fitting modelled predictions of surface deformation to measurements [Dvorak *et al.*, 1997; Dzurisin, 2007]. Such modelling, however, cannot operate without assumptions, and a clear trade-off is present between model precision and the speed of calculation.

Analytical modelling techniques have been the traditional choice for deformation modelling in volcanic systems, due to the speed at which results can be obtained. To function, they typically use a core set of simple assumptions: the Earth's crust

is homogenous and isotropic throughout, deforms elastically when exposed to stress, and has a free surface with no topography. The pioneering Mogi model (Figure 2.1) was developed within this framework, but further assumes that any surface deformation is the product of a point source [Mogi, 1958]. Perturbing this system with a hydrostatic pressure from the point source can produce surface displacements, tilts, and strains. Resulting models can be compared to measured geodetic data to estimate the depth of a pressure source associated with an unrest period [Gudmundsson, 2006; Dzurisin, 2007; Acocella, 2021]. The model was extended to examine pressurized cavities of varying geometries [McTigue, 1987; Yang *et al.*, 1988; Fialko *et al.*, 2001], and with basic topographic corrections [McTigue *et al.*, 1988; Williams *et al.*, 1998, 2000]. Analytical approaches like the Mogi model excel at producing quick, simple results, especially in rapid response to new volcanic deformation episodes [Taylor *et al.*, 2021]. Such haste, however, comes at the expense of accuracy, as the complex nature of the Earth's crust is not considered, especially variations in the mechanical properties and rheology of different crustal components [Currenti *et al.*, 2007; Masterlark, 2007], and the effects of surface topography [Johnson *et al.*, 2019]. The modelling of magmatic systems past basic first-order representations therefore requires additional levels of complexity beyond the capabilities of analytical approaches.

Numerical models differ from analytical methods in that they can be used to consider more complex mathematical problems, such as scenarios with rock layers which vary in their mechanical properties, and that have complex geometries [Masterlark, 2007; Del Negro *et al.*, 2009; Bonaccorso *et al.*, 2013; Currenti, 2014]. The additional level of complexity allows for more accurate representations of crustal conditions, removing some assumptions that analytical methods require. The most common approach taken is Finite Element (FE) modelling, in particular the Finite Element Method (FEM), due to its increased flexibility at solving for heterogeneous materials and complex boundary conditions [Zienkiewicz *et al.*, 2000; Jing *et al.*, 2002]. To conduct advanced FE modelling, substantial knowledge of the volcanic environment is ideally required, such as crustal rheology, heterogeneous mechanical parameters, for example derived from seismic tomography, and digital elevation models (DEMs) for topography [e.g., Hickey *et al.*, 2014]. The FEM splits a model domain down into

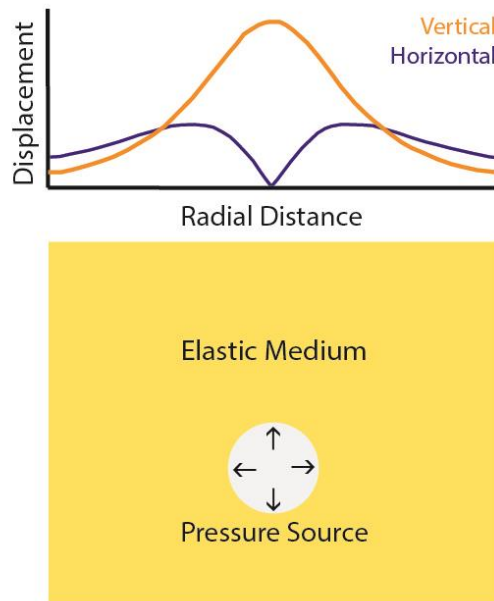


Figure 2.1: ‘Mogi’ model arrangement. The crustal domain is assumed to be uniformly elastic, and resulting vertical and horizontal displacement patterns shown above a free surface [Mogi, 1958].

a collection of smaller elements, which are then joined together at the apex points of each element (called nodes) into a mesh. After material properties and initial and boundary conditions are defined, equations are solved at each individual node, and then combined through the pre-defined mesh to provide a solution across the entire model (Figure 2.2). Altering the size of the meshed elements gives the FEM great adaptability, for example a decrease in element size over areas of specific interest (e.g., volcanic edifices) can improve the resolution of modelled deformation, and produce better representations of more complex shapes, thereby increasing the overall accuracy of the model.

From extensive field campaigns [Gudmundsson, 2011], and seismic tomography surveys [Alanis et al., 2012], volcanic regimes are known to possess a heterogeneous subsurface, which should be reflected in geodetic modelling techniques to produce more accurate results. Successful incorporation of subsurface heterogeneities can be critical to overcoming the limitations of analytical approaches. The addition of heterogeneous characteristics introduces variations in the resultant subsurface stress fields compared to homogeneous domains when magmatic overpressures are applied [Gudmundsson, 2005]. The potential for reductions or amplifications of modelled displacement vectors [e.g., Geyer et al., 2010; Hautmann et al., 2010], highlights the impact that incorporating spatially-variable subsurface physical characteristics can have on

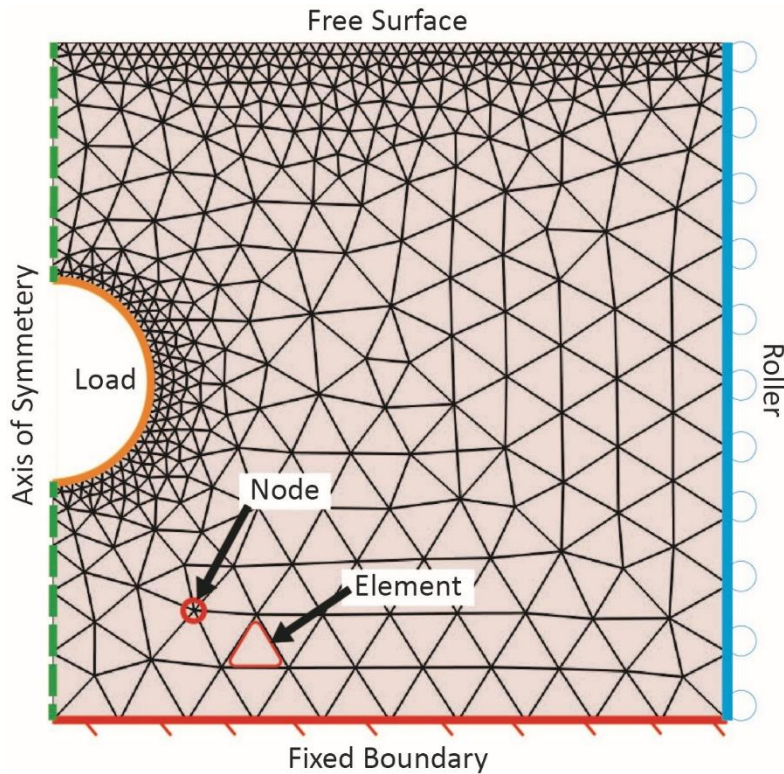


Figure 2.2: Example FEM setup. Higher mesh densities have been applied to the free top surface and immediately adjacent to the load, increasing the resolution of important study areas.

inferred strengths and locations of pressure sources, depending on the level of heterogeneity used for a particular study [e.g., *Currenti et al.*, 2007; *Hickey et al.*, 2016; *Cabaniss et al.*, 2020]. Assessing volcano deformation using FE models has been explored in the past [*Dieterich et al.*, 1975], and now is becoming increasingly common as computational capabilities improve, better enabling the solving of higher complexity problems with greater efficiency [*Masterlark*, 2007]. With the need for better, more sophisticated models growing to match demands of eruption forecasting, numerical modelling techniques must continue to develop, utilizing the ever improving spatial and temporal resolution of deformation observations, to enhance our understanding of the way magmatic systems interact at depth.

2.2.3 Gravity Modelling

Modern studies have highlighted the potential usefulness of volcano gravimetry in active volcanic settings, which can provide insight into subsurface mass distribution changes across varying time periods [*Currenti*, 2018; *Gottsmann et al.*, 2020; *Acocella*, 2021]. Gravity monitoring techniques can identify subsurface magma transport with or without accompanying observable surface deformation

[*Rymer et al.*, 1993; *Bagnardi et al.*, 2014], and can discriminate between different sources of deformation with differing densities, such as magmatic or hydrothermal, that could produce similar surface displacement patterns [*Gottsmann et al.*, 2007; *Battaglia et al.*, 2009; *Fernández et al.*, 2017]. Successfully identifying the cause of surface deformation allows the anticipated hazard to be correctly classified.

The gravitational acceleration at any location on the Earth's surface (980 Gal or 9.8 m/s² on average) is spatially and temporally sensitive to alterations in surface height and subsurface mass distribution, which are common features in volcanic settings [*Dzurisin*, 2007]. Successful removal of other temporal gravity effects, for example ocean tides and varying groundwater levels, leaves behind a residual gravity change, referred to as an anomaly, that can be attributed to topographic or subsurface density changes [*Acocella*, 2021]. To confirm that gravity anomalies are the result of magmatic processes, additional corrections are required to the initial anomaly, such as the correlation between gravity change and measurement elevation (free-air correction) [*Currenti et al.*, 2007], and the density and elevation of rock between the reference level and the measured point (Bouguer correction) [*Rymer et al.*, 2000]. The remaining anomaly can yield information about subsurface mass changes within a volcanic system, potentially indicating magma transfer at depth.

FE modelling using gravitational data has been applied in volcanic settings previously at Mt Etna in Italy [*Currenti et al.*, 2007, 2008; *Currenti*, 2014] and the Corbetti Caldera in Ethiopia [*Gottsmann et al.*, 2020]. In both examples, gravity changes resulting from subsurface density variations are simultaneously calculated along with predicted deformation. The flexibility of the FEM allows each element within a model domain to be assigned a density, creating a full 3D subsurface density profile. This density distribution within the subsurface can be used to calculate the resulting gravity anomaly from the movement of mass within the subsurface, by applying Poisson's differential equation solving for gravitational potential ϕ_g [*Cai et al.*, 2005; *Currenti et al.*, 2007]:

$$\nabla^2 \phi_g = -4\pi G \Delta\rho(x, y, z)$$

where G is the universal gravitational constant ($6.674 \times 10^{-11} \text{m}^3 \text{kg}^{-1} \text{s}^{-2}$), and $\Delta\rho(x, y, z)$ is the change in density across the 3D domain. The gravitational potential at

the domain boundaries is assigned as $\phi_g = 0$ to counter any boundary effects since numerical domains are finite in size. Obtaining the gravitational potential and subsequent Bouguer anomaly relating to subsurface density profiles can be then used to inform on locations and depths of pressure sources within the magmatic system, and resultant volume change during deformation periods [Battaglia *et al.*, 2009; Currenti, 2014].

2.3. The Geology and Volcanism of Japan

2.3.1 The Geography and Geological History of Japan

The nation of Japan is an archipelago comprising over 6,000 islands in East Asia, with the four largest (Honshu, Hokkaido, Kyushu, and Shikoku), accounting for the vast majority of the country's total land area and the bulk of the over 126 million population. Geologically, Japan is a mature island arc located at the intersection of four tectonic plates in the north-western Pacific Ocean (the Pacific, Philippine, North American, and Eurasian) (Figure 2.3) [Satake, 2015]. The Japanese island arc has a long history of subduction, with an estimated 15,000 km of oceanic crust that has subducted beneath Japan over the last 450 million years [Maruyama *et al.*, 1997]. This steady subduction has meant that a large portion of Japan's crust was formed by trench sediment accretion [Nasu *et al.*, 1986], with the accretionary process having contributed an estimated 400 km of material to the Eurasian continent in that same time period [Maruyama *et al.*, 1997]. The shape of the present volcanic arc is the result of back-arc extension between 21 and 14 Ma following a migration of the volcanic front in north-eastern Japan [Tatsumi *et al.*, 1989], forming the Sea of Japan, and resulting in the complete detachment of the Japanese archipelago from the Eurasian continent. New oceanic crust was created, with the rifting causing the clockwise rotation of Shikoku and Southern Honshu by 45 degrees, and a small anti-clockwise rotation of northeast Japan [Ishikawa, 1997].

Modern day tectonic activity continues to be driven by subduction. In the north, the Pacific plate is subducting northwest beneath the North American plate along two trenches, the Kuril and Japan, at 8 cm/yr. The Pacific plate is also subducting beneath the Philippine plate to the south, forming the Izu-Bonin-Mariana arc-trench system. The western edge of the Philippine plate is subducting northeast beneath the North American plate at the Sagami Trough at 4 cm/yr, and

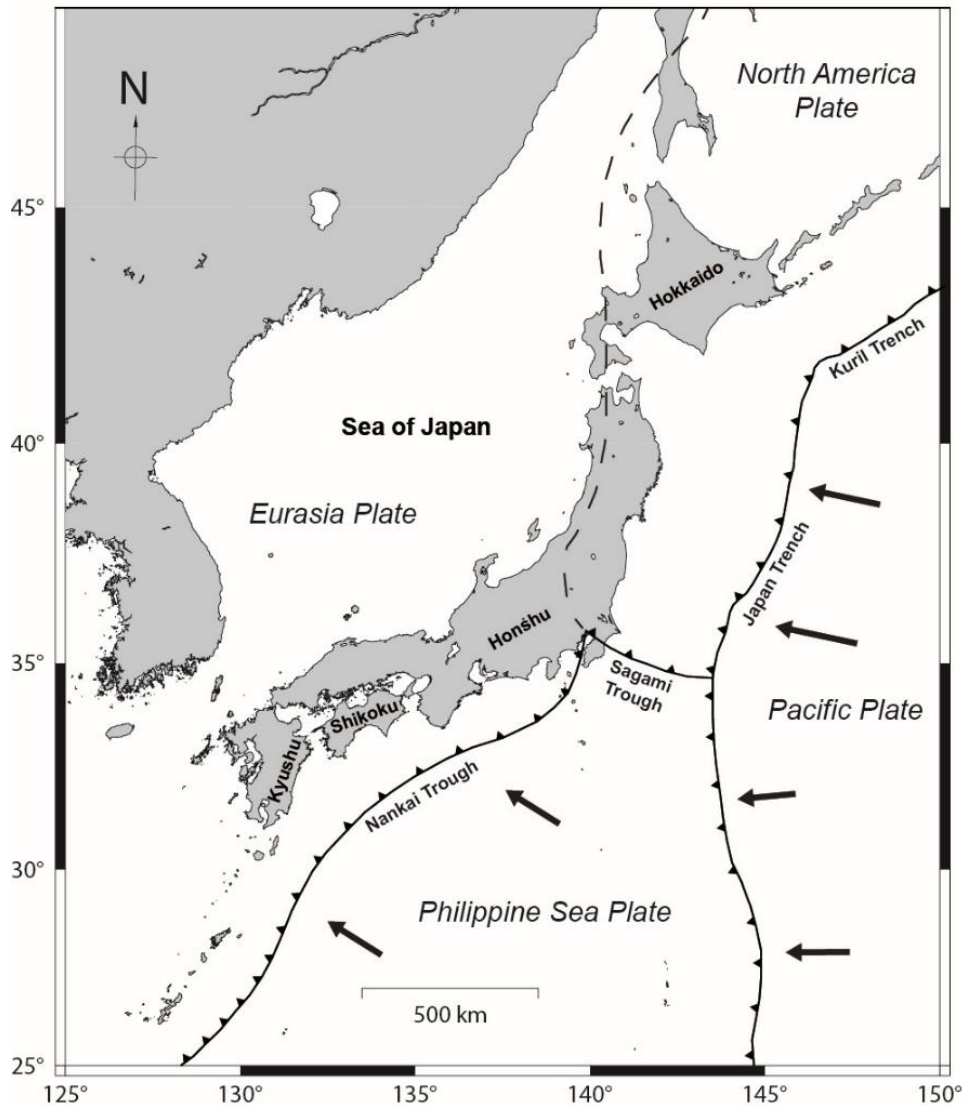


Figure 2.3: Tectonic map of Japan. Overview geographical map of the Japanese archipelago, showing the relationship between the main tectonic plates and margins of the region. The arrows indicate an overall westward plate motion, with the subductive plate margins generating extensive volcanism and tectonic activity throughout the north-western Pacific. Adapted from Satake [2015].

northwest along the Ryukyu Trench and Nankai Trough beneath the Eurasian plate at around 4-7 cm/yr [Sella, 2002]. Seismic activity is common in Japan, with magnitude 7, 8, and 9 earthquakes occurring at average intervals of 3, 23, and 173 years respectively [Satake, 2015]. Large offshore earthquakes can be accompanied by tsunamis, as evidenced by the catastrophic magnitude 9.1 Tōhoku earthquake and tsunami in 2011, which resulted in over 15,800 fatalities [Mori et al., 2014]. Volcanism is a key feature of Japan's past and present, with the archipelago being home to over 100 active volcanoes, accounting for around 10% of the world's total. Volcanoes are dispersed throughout the islands, except for Shikoku and southern Honshu, with the main volcanic landforms consisting of

stratovolcanoes and calderas. Due to the proximity of population centres, over 50 volcanoes are under 24-hour surveillance. The most recent significant eruptions were in 1991 at Mount Unzen and in 2014 at Mount Ontake, which caused 43 and 63 fatalities respectively [Yamamoto, 1993; Kaneko, 2016]. Due to a high percentage of mountainous terrain, the Japanese population is concentrated in dense urban, and typically coastal, environments. Some of these population centers are near active volcanoes, with five cities, Tokyo, Sapporo, Nagoya, Osaka, and Fukuoka (with a combined population of 22.44 million), being considered in the Top 20 most at risk cities from a volcanic eruption [Oramas-Dorta et al., 2019]. Active monitoring and safety precautions, therefore, are of the utmost importance to minimize fatalities and loss of livelihoods, property, and infrastructure during periods of disaster.

2.3.2 The History of Kyushu and Sakurajima

Kyushu is the third largest of the Japanese archipelago's four main islands, and has an especially rich volcanic history; the past 1 Ma alone have seen over 1,000 km³ of dacitic and andesitic lavas being erupted [Aramaki, 1984]. Volcanism in Kyushu can be separated into three regions to describe its volcanic history: the north-western, central, and southern (Figure 2.4). The north-western region has seen episodic back-arc volcanism, producing both monogenetic and polygenetic volcanoes, and flood basalts. In contrast, the central region has long-lived volcanism, with a range of activity from calderas to lava plateaus. The southern region, along the arc front, has hosted widespread lava eruptions and calderas within the last 0.3 Ma [Kamata et al., 1999]. Volcanism since 0.3 Ma has also been noticeably more explosive when compared to activity prior, up to 2 Ma [Taira, 2001]. Current volcanism occurs mostly within two large grabens: the Beppu-Shimabara graben in the central region, and the Kagoshima graben in the southern region (Figure 2.4). The Beppu-Shimabara graben is at the intersection between extensional and subductive tectonic regimes, and represents the terminus of the Okinawa Trough to the southwest [Tada, 1985], and is home to the volcanic centres of Unzen and Aso. Further towards the southeast, the Kagoshima graben contains the large Kirishima, Aira, and Ata calderas from north to south, as well as the submarine Kikai caldera 50 km offshore to the south, which was the source of the largest Holocene eruption in Japan (7.3 ka) [Maeno et al., 2007].

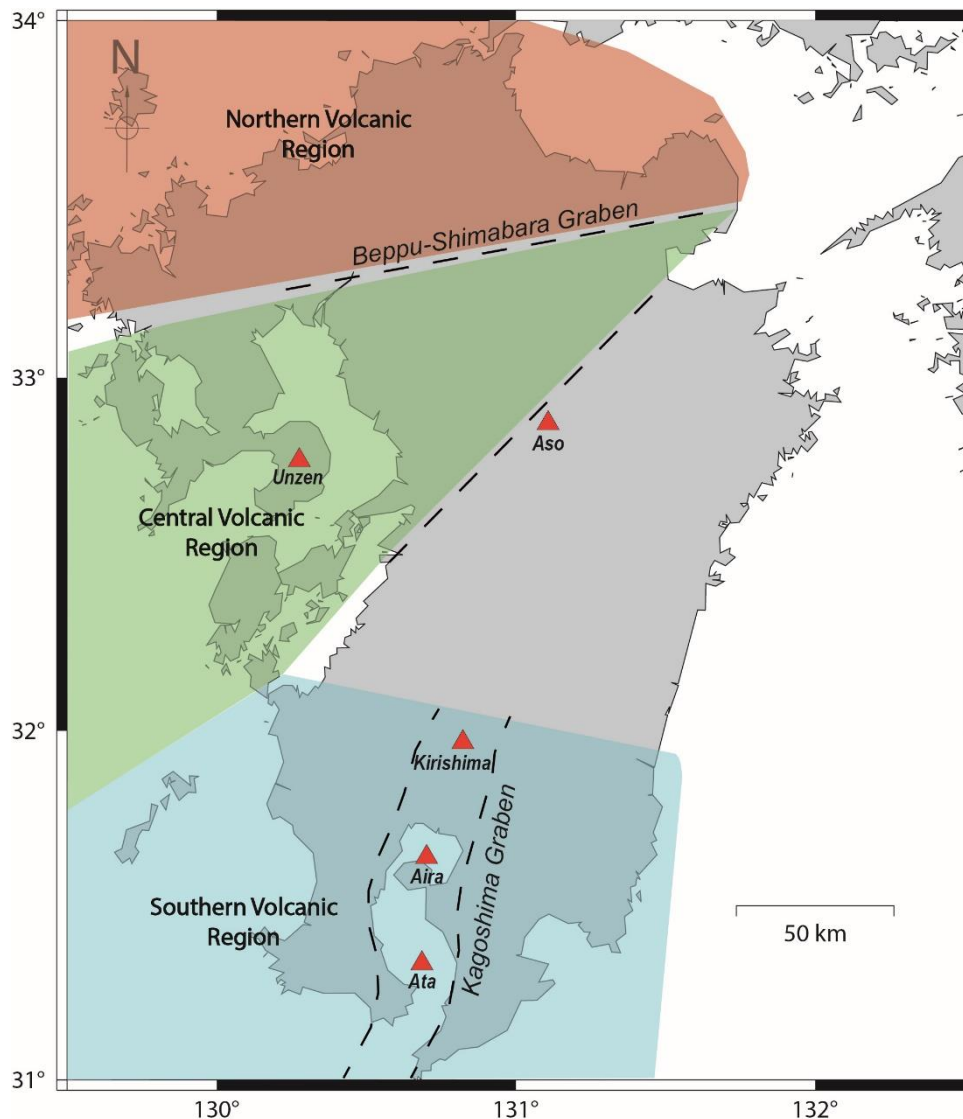


Figure 2.4: Volcanic Region map of Kyushu. Graben extents are show by dashed line, with main volcanic centers and calderas shown by red triangles.

Aira caldera, located in southern Kyushu, was formed during a VEI 7 Plinian event around 29,000 years ago [Aramaki, 1984; Okuno, 2002], with the 17 km by 23 km caldera now part of Kagoshima Bay (Figure 2.5). Sakurajima volcano, the main active vent of the caldera, is located on the southern rim of the caldera. Primarily of andesitic composition, Sakurajima volcano has two central cones, Kitadake and Minamidake, which have erupted repeatedly over the past 600 years of recorded history, as well as numerous parasitic vents and craters surrounding the main peaks. Since 1955, small-scale vulcanian eruptions have become an almost daily occurrence from Minamidake and a small parasitic vent 500 m east of Minamidake, Showa crater [Nakagawa, 2011; Iguchi, 2013], with the high levels of activity meaning Sakurajima is Japan's most active volcano. The process of building the volcano we see today occurred in three stages. The

earliest activity occurred between 26-24 ka, known as the Old Kitadake, followed by New Kitadake from 13-5 ka, and finally Minamidake, which is active today [Kobayashi *et al.*, 2002]. The activity of the volcano has continually shifted south over time, as evidenced by the relative age difference and current activity levels of Sakurajima's main peaks. Numerous parasitic vents surround the central summit, and have been the source of the regular activity observed in the historical record since AD 708, with three distinct periods of VEI 4-5 Plinian eruptions: the Bummei (1471-1476), An-ei (1779-1782), and Taisho (1914-1915) [Yamaguchi, 1975; Kobayashi, 2013]. Each of the three major eruptions produced a pair of parasitic vents on opposite sides to the central summit, with new vents formed at an increasing radial distance as the eruption progressed [Yamaguchi, 1975; Yokoyama, 2013]. The Taisho eruption of 1914 produced 0.52 km³ of pumice and ash, and 1.34 km³ of lava [Ishihara *et al.*, 1981], which resulted in the then island being connected to Osumi Peninsula to the southeast by a narrow isthmus of lava [Todde *et al.*, 2017]. Representing the largest eruption of the twentieth century in Japan, the 1914 Taisho eruption highlights the potential for future eruptions of Sakurajima, and with the population around the volcano having grown significantly in the past 100 years, monitoring of the volcano is essential.

2.3.3 Sakurajima Volcano Monitoring and Modelling History

The proximity of Sakurajima to the over 600,000 residents of Kagoshima city (8 km west), and to the 5,000 located on the island itself, means Sakurajima poses a significant threat [Hickey *et al.*, 2016; Araya *et al.*, 2019]. In the 1990's, Sakurajima was declared a "Decade Volcano" by the International Association of Volcanology and Chemistry of the Earth's Interior (IAVCEI), which makes it one of the 16 high-risk volcanoes around the world to be intensively studied, further including Merapi in Indonesia, Rainier in the USA, and Unzen, also on the island of Kyushu [IAVCEI, 1994]. Sakurajima is continuously monitored, with eruption reports being produced by the Volcanic Ash Advisory Center in Tokyo, that detail eruption time and height of any corresponding ash plumes. Growing concerns of a future large scale, Taisho-equivalent eruption, has led to a pressing need for research into the driving forces behind the volcano's constant activity [Hickey *et al.*, 2016], with numerous deformation models having being conducted to analyse the subsurface magmatic system.

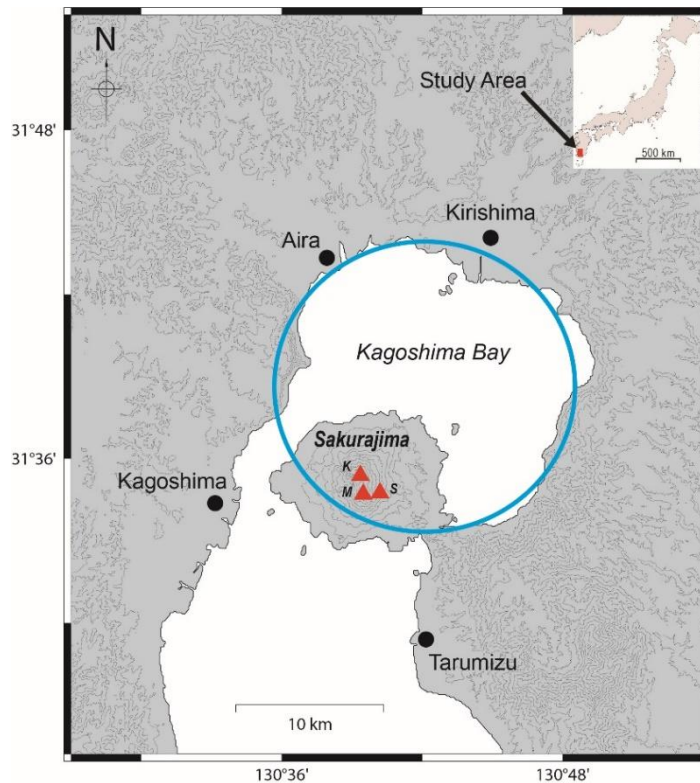


Figure 2.5: Kagoshima Bay and Sakurajima volcano locations. The blue circle shows the extent of Aira caldera, with red triangles K (Kitadake), M (Minamidake), and S (Showa crater) representing the peaks and vents of the volcano.

Long-term deformation data stretches back to 1892 (Figure 2.6), when the first levelling survey was conducted [Omori, 1916; Iguchi, 2013]. Repeat surveys after the Taisho eruption of 1914 suggested that significant ground subsidence accompanied the eruption, with a maximum subsidence of 2 m, and a distinctive concentric deformation pattern along Kagoshima Bay [Omori, 1916]. From analytical modelling using the deformation patterns observed, a deflation source at a depth of 10 ± 1 km was interpreted, centered beneath Aira caldera [Mogi, 1958]. The fact that deformation was concentric around the whole of Kagoshima Bay, rather than closer to Sakurajima where the eruption occurred, implies that the magmatic systems of Sakurajima and Aira caldera are closely linked. Following the start of vulcanian activity at Minamidake in October 1955, precise levelling surveys were more regularly conducted around Sakurajima [Hotta *et al.*, 2016]. Significant displacements of Sakurajima compared to Aira caldera prior to eruptive activity between 1974-1992 [Ishihara *et al.*, 1978] implied multiple pressure sources were present in the system. This deformation, centered on a region northeast of Sakurajima, was modelled as having two sources at 10 km and 3 km depth, beneath Aira caldera and the Minamidake vent, respectively

[Eto, 1989]. Modelling after a period of ground deformation between 2006 and 2011, accompanied by increased activity from the Showa crater, again suggested two pressure sources, this time at 12 km and 5 km beneath Aira caldera and Kitadake [Iguchi *et al.*, 2013], reinforcing the hypothesis of multiple pressure sources. A similar pattern of deformation accompanied high explosivity eruptions from Showa crater between late 2011 and early 2012 suggested three sources in the system (9.6 km beneath Aira caldera, 3.3 km beneath Kitadake, and 0.7 km beneath Minamidake), using combined with GPS, tilt, and strain data [Hotta *et al.*, 2016]. The additional third source was inferred from the inflation of a water-tube tiltmeter situated south of Minamidake in July 2010, which only showed signs of deflation a full month later than the rest of the network, implying magma migration between Kitadake and Minamidake [Hotta *et al.*, 2016].

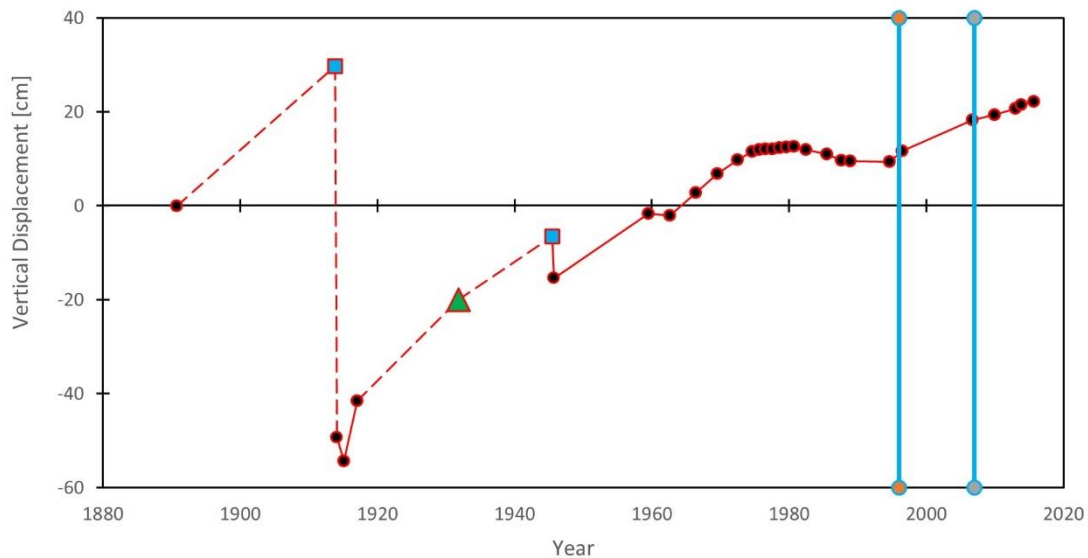


Figure 2.6: Deformation history of Aira caldera. Green triangle and blue squares represent inferred levels based on extrapolation from previous benchmarks or tidal gauge data, with black circles from levelling surveys. The 1996 – 2007 deformation period is confined within the blue lines. Adapted from Hickey *et al.* [2016].

Despite the limitations of models that assume a homogeneous subsurface, the foundation for the majority of geodetic models of Aira and Sakurajima use a point pressure, analytical modelling approach [Mogi, 1958]. However, by neglecting the complexities inherent in the Earth's subsurface, the chance of producing accurate models for a deeper understanding of the Aira caldera magmatic system is decreased [Currenti *et al.*, 2007; Hickey *et al.*, 2016]. Since the active monitoring of volcanoes that pose a threat to life, such as Sakurajima, is a high priority,

geodetic modelling efforts should be more complex to better interpret deformation events for eruption forecasting and subsequent hazard management.

To date, FE modelling has rarely been applied to Sakurajima, with most models being conducted using analytical methods. *Hickey et al.* [2016] conducted FE modelling using GPS data from 1996 to 2007, to test the impact of crustal heterogeneity and surface topography and bathymetry on the models, and to obtain the optimal parameters of the main pressure source. The resulting best fit source was an oblate spheroid, at a depth of around 13 km beneath the north-eastern part of Aira caldera, proximal to the Wakamiko depression and its active fumaroles [*Hickey et al.*, 2016]; results that significantly differed from an analytical study of the same deformation period (11 km depth just north of Sakurajima). Only one pressure source was used for the FE study, with the resulting modelled deformation profile showing notable misfits around Sakurajima itself. *Hickey et al.* [2016] suggested these misfits could be explained by a connective magma pathway between a deep and a shallow reservoir, such as a dyke, on north-eastern region of the volcano.

Most of the previous modelling work of Sakurajima shows the preference of analytical deformation models, with a growing consensus that multiple pressure sources are present. However, these studies have not addressed the known limitations with analytical methods regarding the inclusions of subsurface heterogeneities. Inaccurate estimates of source location and magnitude from purely analytical methods can be improved by including subsurface heterogeneity, inelastic rheologies, the topography of the area in question, and modelling resultant displacements using higher capacity numerical methods. Despite the consensus view that the Aira caldera magmatic system has multiple pressure sources, this hypothesis has never been tested using numerical techniques. Improved modelling of a multiple pressure source system beneath a 3D volcanic edifice requires an understanding of how pressure sources interact. A preliminary 2D study can provide information of the effects of shallow source shape, size, overpressure, and depth, whilst also assessing the scale of which deeper, larger storage reservoirs can obscure displacements resulting from smaller, shallower reservoirs. Results from the 2D study are then applied to Sakurajima volcano in full 3D, utilizing the same deformation period as *Iguchi et al.* [2008] and *Hickey et al.* [2016], to compare between the modelled

displacement vectors of single and multiple pressure sources, and which arrangement better replicates the measured displacements.

Chapter 3:
Shallow Pressure Source
Contributions to Surface
Displacement Patterns in a Stacked
Magma Reservoir Setup

3.1 Introduction

Ascent, migration, and accumulation of magma within volcanic systems transfers stress and strain through the Earth's crust [Gudmundsson, 2012]. This transfer can often cause surface displacements, which can be indicative of the location and magnitude of shallow magmatic storage regions [Dvorak *et al.*, 1997; Poland *et al.*, 2006; Parks *et al.*, 2012; Fernández *et al.*, 2017]. First order estimates of magma storage locations and magnitudes can be attained using basic analytical models, aiming to match modelled predictions to measured displacements [Mogi, 1958; McTigue, 1987; Yang *et al.*, 1988; Fialko *et al.*, 2001]. Attaining quick results however comes with reduced accuracy, as complexities within the Earth's crust are not considered, such as realistic subsurface conditions [Currenti *et al.*, 2007; Masterlark, 2007; Hickey *et al.*, 2020], or surface topographies [Johnson *et al.*, 2019]. Numerical methods, utilizing elevated computational capacities, can create a more realistic heterogeneous representation of the volcanic system in question [Del Negro *et al.*, 2009; Gregg *et al.*, 2013]. Regardless of the method used, the objective of modelling remains the same: to aid eruption forecasting and hazard assessments by inferring the location and scale of causative magmatic storage systems at depth [Dvorak *et al.*, 1997; Poland *et al.*, 2006; Parks *et al.*, 2012; Fernández *et al.*, 2017].

Magmatic reservoirs have historically been modelled as point sources [e.g., Mogi, 1958] or cavities of varying geometries [McTigue, 1987; Yang *et al.*, 1988; Fialko *et al.*, 2001; Hickey *et al.*, 2020]. Modelling multiple magmatic sources usually requires vertically stacking of chambers, or stacking with a lateral offset [Tiamo *et al.*, 2000; Kohno *et al.*, 2008]. Surface displacements in single magmatic source models can be assumed to emanate from that single source, leading to direct overpressure, size, location, and depth estimates [e.g., Mogi, 1958]. Multiple magmatic source arrangements complicate this deductive process as displacements are often assumed to be the combined result of all the sources within the system [Pascal *et al.*, 2014]. Determining potential locations and magnitudes of secondary, shallower pressure sources compared to a larger, primary source is dependent on the accuracy of the type of geodetic measuring instrumentation used, with small parameter differences likely undetectable with low instrument resolution, directly impacting potential eruption forecasts and hazard assessments.

Here, a range of overpressures, depths, shapes, and sizes of secondary, shallow magmatic sources are tested in a pseudo-3D heterogeneous model domain, in combination with a fixed large deep source acting as a primary magma reservoir. Independently varying the parameters in the shallow source allows their effects on the surface deformation field to be analysed, and to determine which parameters result in the largest surface change, while also highlighting how much a deep pressure source can dominate volcanic surface displacements, and potentially obscure the presence of smaller pressure sources.

3.2 Methods

3.2.1 Model Setup

Computation of models for this study was conducted using the solid mechanics and CAD import modules of COMSOL Multiphysics v5.3.

Geometry

A 50 km x 50 km model domain was constructed, with the top axis representing a flat topography, and the rest of the domain below representing the subsurface. The free top and fixed base boundaries constrain vertical aspects of the domain, with horizontal extents contained within a vertically aligned roller on one axis, and an axis of symmetry on the other, creating a pseudo-3D model, with a 2 km thick Infinite Element Domain (IED) wrapped around the horizontal and vertical extents (Figure 3.1). An IED numerically extends the outer constraints of a finite model in the assigned directions, infinitely increasing the separation between the interest area of the model and any boundary conditions [Hickey *et al.*, 2014], thereby reducing the additional computational time that would be required for a larger model to remove boundary effects.

The two vertically stacked cavities were added on the axis of symmetry, resulting in a 100 km diameter pseudo-3D cylinder encasing the cavities within a 50 km deep domain below the center point. Finally, the application of boundary loads normal to the cavity surfaces simulated magmatic overpressures on the adjacent crust. Each model iteration had around 30,000 domain elements, with an increased mesh density surrounding the cavities and along the surface to improve modelled displacement precision.

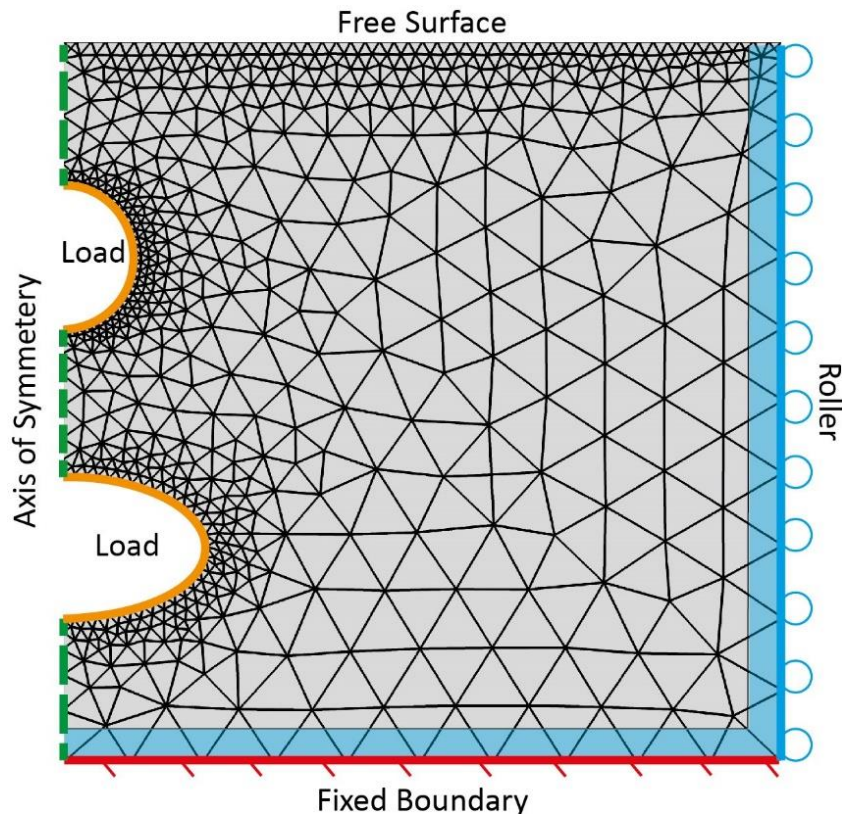


Figure 3.1: Double pressure source FEM arrangement. Boundary loads (orange lines) are applied to the two cavities, which represent the magmatic sources, and vertically stacked on an axis of symmetry (green line). An Infinite Element Domain is shown by the blue regions adjacent to the lateral boundary roller and the fixed zero-displacement base (red line). Both the mesh and source sizes are not to scale.

Model Physics

Models included in this study employ linear elasticity throughout the domain, which assumes strain is directly proportional stress, and that deformation occurs instantaneously when a load is applied [Ranalli, 1995; Hickey *et al.*, 2013]. Non-elastic rheologies were excluded to enable modelling work to focus on the spatial deformation patterns instead of time-dependant phenomena. A constant Poisson's Ratio of 0.25 and density of 2700 kg/m^3 was chosen for all model domains to represent typical values of crustal rock [Komazawa *et al.*, 2008; Gudmundsson, 2009].

Rough subsurface heterogeneity was incorporated into the models by varying the Young's Modulus (YM) of the model domain, defining it as a function of depth along a constant gradient (Figure 3.2). A YM value of 20 GPa was assigned to the surface, increasing at 0.6 GPa/km to a maximum value of 50 GPa at 50 km. Defining the YM of the material as a perfectly linear function is not entirely realistic

in a geological setting, but provides a rough heterogeneity to a hypothetical system, thereby improving on a purely homogeneous domain.

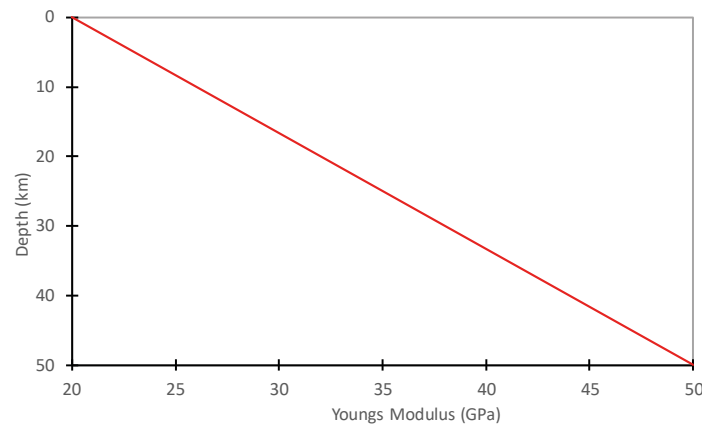


Figure 3.2: Basic modelled subsurface heterogeneity. Linear Young's Modulus variance with depth used throughout the model domain.

This chapter focused purely on the parameter variance of secondary shallow pressure sources rather than comparing between homogenous and heterogenous modelling methods. The deficiencies in homogeneous modelling approaches have been extensively explored in previous studies, highlighting the requirement for oversimplification and assumptions of subsurface mechanical properties [Currenti *et al.*, 2007; Masterlark, 2007], and the displacement vector variance of each domain type during the application of magmatic overpressures [Gudmundsson, 2005; Geyer *et al.*, 2010; Hautmann *et al.*, 2010]. Analytical methods also struggle to account for multiple pressure sources with close proximities to each other [Pascal *et al.*, 2014], which could hamper efforts to test homogenous equivalents the models used in this chapter, hence no homogenous models were constructed.

3.2.2 Modelling Approach

To test the relationship between surface displacement patterns and multiple pressure source systems, displacements from a single source model were obtained first. By establishing a baseline deformation of a single source, subsequent differences in the displacement patterns and magnitudes from the addition of a secondary source can be directly analysed. To act as the deep pressure source, an oblate cavity was added at a depth of 10 km, with axes 3 km x 1 km, and was assigned a pressurized boundary load of 10 MPa, simulating the effects of an overpressure. The resulting uplift on the flat surface was measured,

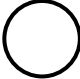
and serves as the foundation for subsequent iterations.

With the deep oblate source parameters kept constant throughout, a shallow source was added to the domain. Overpressure, volume, and depth values of the shallow source ranged between 2 – 10 MPa, 0.52 – 14.14 km³, and 3 – 7 km (Table 3.1). Spheroids of several eccentricities were tested, with oblate, prolate and spherical shapes used. To better enable comparisons between the different source shapes, the volumes of the oblate and prolate sources were set to be equal with the volume of an equivalent spherical source, with axes lengths calculated by defining ratios (2:1, 1:1, 1:2) between semi-major and semi-minor axes of each shape (Table 3.2). Separate models were constructed for each for the three source shapes used (oblate, prolate, spherical).

Sensitivity tests of individual parameters was accompanied by median values of the remaining parameters not being analysed. For example, modelling of the full range of overpressure values (2 – 10 MPa) used shallow source depths and volumes of 5 km and 4.19 km³, respectively. Variance of only one shallow parameter at a time allowed for simple analysis of how that parameter affected displacement magnitudes. Both vertical and horizontal components of the resulting displacements were extracted for analysis, with the uplift contribution of each shallow source iteration calculated by subtracting the baseline single source displacement from the double source displacement, producing an “displacement difference” value. Overall, 90 different “displacement difference” values were calculated across the full range of shapes, overpressures, depths, and volumes.

<i>Overpressures (MPa)</i>	<i>Volumes (km³)</i>	<i>Depths (km)</i>
2	0.52	3
4	1.77	4
6	4.19	5
8	8.18	6
10	14.14	7

Table 3.1: Full range of shallow source parameters tested. Median values used during parameter sensitivity tests are highlighted.

	<i>R (km)</i>	<i>Semi-Major (km)</i>	<i>Semi-Minor (km)</i>	<i>Volume (km³)</i>
<i>Spherical</i>	0.50	-	-	0.52
	0.75	-	-	1.77
	1.00	-	-	4.19
	1.25	-	-	8.18
	1.50	-	-	14.14



<i>Oblate 1:2</i> 	-	0.63	0.31	0.52
	-	0.94	0.47	1.77
	-	1.26	0.63	4.19
	-	1.57	0.79	8.18
	-	1.89	0.94	14.14
<i>Prolate 2:1</i> 	-	0.40	0.79	0.52
	-	0.60	1.19	1.77
	-	0.79	1.59	4.19
	-	0.99	1.98	8.18
	-	1.19	2.38	14.14

Table 3.2: Tested range of shallow source shape, volumes, and axes lengths. Axes lengths for different shapes are calculated by matching the volume of the equivalent sphere, using defined axis ratios for each shape.

3.3 Results

The objective of this modelling is to assess the uplift differences between double and single source magmatic systems, and to determine the influence of shallow source parameters, such as overpressure, volume, and depth, on the resulting deformation field. To do this, it is important to consider changes whilst being mindful of typical error margins in modern day deformation measuring instrumentation, as this will indicate whether any changes would be discernible during data collection. On average, the precision of GPS measuring techniques is around 10 mm vertically and a few mm horizontally [Dzurisin, 2007]. We take the lower precision value of 10 mm as a threshold value throughout this study. A displacement difference of less than the 10 mm minimum value means geodetic techniques would not be able distinguish the number of pressure sources within a particular volcanic system.

3.3.1 Depth

Across the full range of depths tested (3 – 7 km), the maximum displacements are observed at the shallowest depth of 3 km for all three source shapes (oblate, prolate, and spherical), and in both vertical and horizontal components. (Figure 3.3). Oblate sources produce the greatest magnitudes, with maximum vertical and horizontal displacement differences of 85 mm and 27 mm respectively, compared to the base single source model. Prolate sources show the smallest displacement differences, peaking at 22 mm and 17 mm for vertical and horizontal components. Of the five depths modelled, only the shallowest three depths (3 km, 4 km, and 5 km) produce displacement differences greater than

the threshold of 10 mm, with 50% of the source shape and displacement component combinations only exceeding the 10 mm threshold when the shallowest depth of 3 km is used.

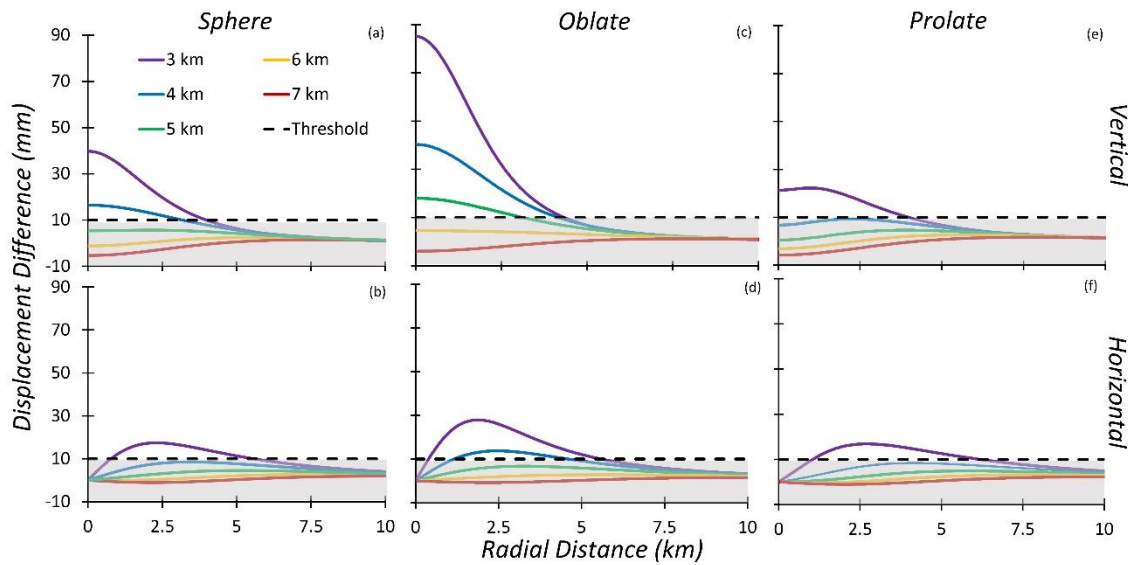


Figure 3.3: Displacement difference values when varying depth. Displacement differences from spherical (a & b), oblate (c & d), and prolate (e & f) shaped shallow sources. Vertical (a, c, & e) and horizontal (b, d, & f) direction components are arranged by row. Depths used are colour coded using the legend in (a), with the threshold displacement shown with the dashed black line and grey shading.

3.3.2 Volume

Maximum displacement differences are produced with the inclusion of the largest shallow source (14.14 km^3) for all three shapes modelled, with an oblate shape yielding the highest displacement difference values of 69 mm and 25 mm for vertical and horizontal components. Prolate sources generate the smallest displacement differences, with values of 17 mm (vertical and horizontal) when employing the maximum volume (Figure 3.4). Only the three largest volumes (4.19 km^3 , 8.18 km^3 , and 14.14 km^3) produce displacement differences that exceed the 10 mm threshold. Like the depth results, 50% of the shape and deformation component combinations only exceed the 10 mm threshold with the addition of the largest volume (14.14 km^3).

3.3.3 Overpressure

The largest displacement difference values are produced from the highest shallow source overpressure value of 10 MPa, with an oblate shaped source generating peak values of 53 mm and 18 mm for vertical and horizontal

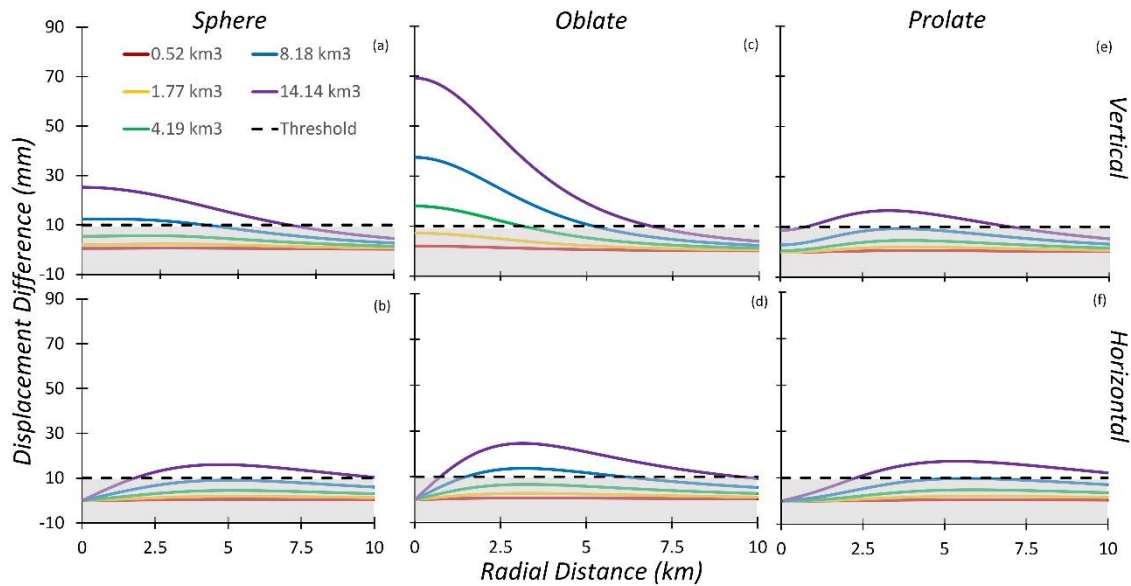


Figure 3.4: Displacement difference values when varying volume. Displacement differences from spherical (a & b), oblate (c & d), and prolate (e & f) shaped shallow sources. Vertical (a, c, & e) and horizontal (b, d, & f) direction components are arranged by row. Volumes used are colour coded using the legend in (a), with the threshold displacement shown with the dashed black line and grey shading.

components. An equivalently overpressurized shallow prolate source yields the smallest displacement differences of 12 mm and 10 mm for vertical and horizontal components (Figure 3.5). Comparable to both the depth and overpressure results, 50% of deformation component and shape combinations only exceed the threshold 10 mm uplift difference when the largest overpressure (10 MPa) is applied to the shallow source. However, two of these, measuring horizontal displacements of spherical and prolate shallow sources, only exceed the 10 mm threshold by 0.87 mm and 0.35 mm respectively, even with the highest 10 MPa overpressure.

3.4 Discussion

3.4.1 Source Shape

For the three shallow source shapes tested (oblate, prolate, and spherical), oblate sources produce the greatest vertical displacement differences compared against the base single deep source in every tested example. This is expected due to the overall greater relative proportion of vertical displacement from oblate-shaped sources, produced by the larger upward-facing source surface area [Okada, 1992; Dzurisin, 2007; Hickey *et al.*, 2013]. Shallow prolate sources by contrast

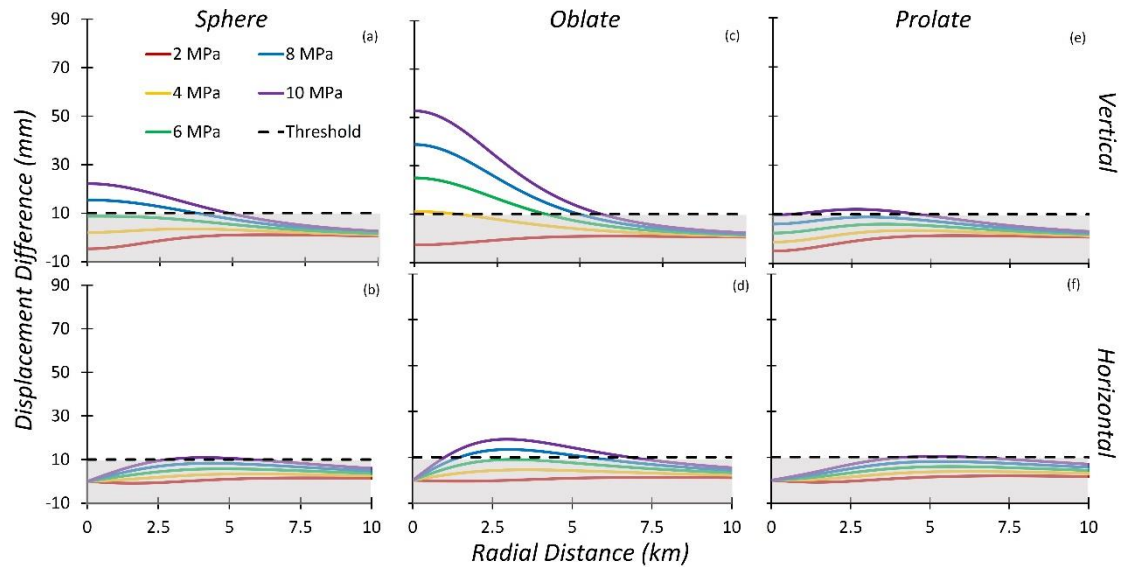


Figure 3.5: Displacement difference values when varying overpressure. Displacement differences from spherical (a & b), oblate (c & d), and prolate (e & f) shaped shallow sources. Vertical (a, c, & e) and horizontal (b, d, & f) direction components are arranged by row. Overpressures used are colour coded using the legend in (a), with the threshold displacement shown with the dashed black line and grey shading.

produce the smallest vertical displacement differences compared to the base single source model, as the smaller upward-facing surface area transfers relatively more stress horizontally than vertically; this is evidenced by the fact the maximum uplift difference values are not found directly above the stacked pressure sources, with this off-centre maximum displacement also observable in analytical methods [Bonaccorso *et al.*, 1999; Dzurisin, 2007].

3.4.2 Direction Component

Across all parameter combinations, vertical components show significantly greater displacement difference magnitudes when compared to the horizontal equivalents (Figure 3.6). Vertical components typically produce the highest magnitudes directly above the sources, falling away sharply with distance from a center point. The largest horizontal displacement magnitudes conversely occur away from the central point, on average 2 – 7 km away. The largest radial displacement difference observed is from a 3 km deep shallow oblate source, with a value of 28 mm, 1.9 km from the center of the model. Unlike vertical displacements, the order of oblate, spherical, and prolate uplift differences does not remain constant through the full parameter range. Oblate sources still produce the largest observed radial displacement difference across the explored

depth, overpressure, and volume variables, however, spherical and prolate sources are not consistent. The maximum volume of 14.14 km^3 produces displacement differences values of 25 mm, 17 mm, and 16 mm (3.15 km, 5.30 km, 4.75 km radial distances) for oblate, prolate, and spherical respectively, with the spherical source producing the smallest displacement difference. This variability shows the importance of testing different source shapes alongside depth, overpressure, and volume parameters for shallow pressure sources.

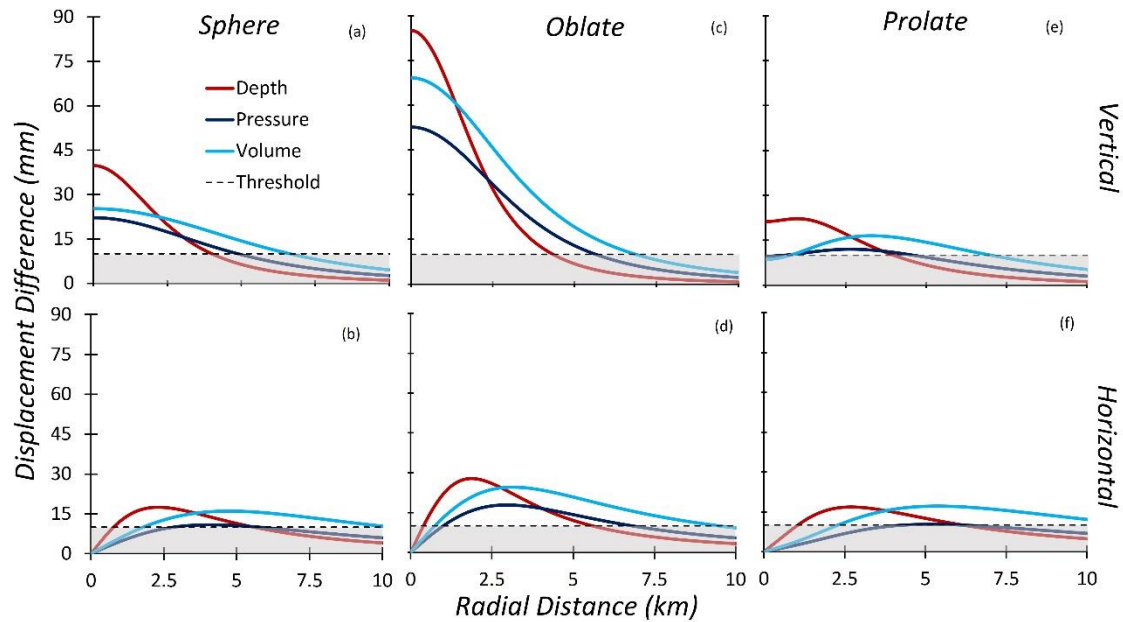


Figure 3.6: Maximum modelled displacements. Largest displacement differences from spherical (a & b), oblate (c & d), and prolate (e & f) shaped shallow sources. Vertical (a, c, & e) and horizontal (b, d, & f) direction components are arranged by row. Parameters used are colour coded using the legend in (a), and represent the highest observed uplift differences from shallow source depth (3 km), overpressure (10 MPa), and volume (14.14 km^3). The threshold displacement of 10 mm is shown by the grey shading.

3.4.3 Implications

Maintaining a constant deep pressure source, whilst varying overpressures, depths, volumes, and shapes of a secondary shallow source, allows for the displacement contribution from a shallow pressure source to be distinguished. A threshold difference of 10 mm was used to realistically account for errors in geodetic measurements, with only shallow source arrangements exceeding this 10 mm threshold being distinguishable from a single source model. It should be noted that in every double magmatic source arrangement in this study, the parameters of the deep source were kept constant. Whilst allowing easy analysis

of shallow source parameters, the modelled results only reflect the deep source setup used. Altering the depth, volume, overpressure, and shape of the deep source will alter the displacement contributions from the major source. A shallower, larger, or more overpressurized main reservoir is likely to produce greater surface deformation, further dominating the modelled displacement patterns, and increasing the difficulty of discerning shallow pressure source contributions.

Across the three different source shapes (oblate, prolate, spherical), shallow pressure sources with overpressures less than 6 MPa, volumes less than 4.19 km³, and depths greater than 5 km, fail to produce displacement difference values that exceed the threshold mark of 10 mm. The failure to exceed the 10 mm threshold below these shallow source parameters implies any displacement contribution of the shallow source is undetectable compared to the displacements caused by the larger, deeper source within the arrangement. The potential inability to detect shallow magmatic storage reservoirs within a magmatic system could have consequences for eruption forecasting and hazard assessment. Failure of a shallow reservoir due to high levels of internal overpressure [Ranalli, 1995], typically between 0.5 – 9 MPa [Gudmundsson, 2011], can lead to the upward propagation of a dyke, erupting at the surface. The reduced vertical distance that any propagating dyke would have to travel from a shallow reservoir, compared to a deeper reservoir, would enable the dyke to reach its potential eruptive location faster, possibly producing an eruption with reduced warning times, as perceived from geodetic monitoring techniques. The chance for undetected shallow reservoirs to produce surprise eruptions, despite the possibility for such eruptions to be small in scale due to the lower volume of migrating magma, is a potential concern.

3.5 Limitations

The vertically stacked arrangement of the pressurized cavities generates the maximum vertical displacement differences directly above the pressure sources, except for the prolate shaped sources. Accounting for a horizontal offset between shallow and deep storage reservoirs would change the location on the surface where the maximum displacement difference values are observed, rather than just being located above the major reservoir. Whilst deep, low overpressure, and

small secondary shallow sources produce sub-threshold displacement differences, this is unlikely to be fully representative of magmatic systems with a horizontal offset between pressure sources. Magmatic sources within volcanic systems are typically horizontally offset from the main eruptive vent [*Ebmeier et al.*, 2018], and geodetic observations can also show a horizontal offset between pressure sources [*Hotta et al.*, 2016; *Araya et al.*, 2019]. Lateral offsets are not possible to replicate in the pseudo-3D approach used here; a full 3D geometry would be required.

Tiltmeters are commonly used in modern volcanic monitoring as an alternative way of measuring surface displacement alterations of a volcanic edifice [*Dzurisin*, 1992; *Fernández et al.*, 2017; *Johnson et al.*, 2019]. Whilst this study focused on extracting displacement values from the models, the merits of analysing the change of slope angle are worth considering, due to the potential to characterize deformation profiles with off-centre maximum displacement values, such as those observed with a shallow prolate source, and in horizontal displacements.

Modelling work conducted here used a first-order subsurface heterogeneity to simulate mechanical variance within the Earth's crust, with the primary focus on assessing how changing shallow pressure source parameters altered the resulting surface deformation profiles. Therefore, the impact of the heterogeneity used on the resulting profiles was not analysed, along with the potential differences to a homogenous domain.

Understanding the first order impacts on surface displacements from changes to shallow source depths, overpressures, and volumes is viable using 2D methods, but is best used to establish a foundation to build upon in a full 3D geometry of a volcanic system. Fully modelling a volcanic system in three-dimensional space produces a more realistic representation of magmatic systems, achieving more accurate interpretations of volcanic deformation through geodetic modelling.

3.6 Conclusions

The modelling of a 2D-axisymmetric, vertically stacked magmatic system, was conducted to better understand alterations of shallow pressure source overpressures, depths, volumes, and shapes, in a double magmatic source system. Utilizing rough subsurface heterogeneity from a linear Young's Modulus

in the model domain, displacements between a base, single source deformation model and double source model were calculated. The double source models featured a secondary shallow pressure source with a range of shapes, overpressures, depths, and volumes. The resulting displacements between single and double source models were compared using a “displacement difference” and a threshold error margin of 10 mm, representative of modern geodetic monitoring equipment resolution, to analyse whether displacements from the shallower source can be determined in the resulting deformation profiles.

For the three source parameters tested (overpressure, depth, volume), the greatest displacements are observed for sources at the shallowest depth (3 km), or with the highest overpressure (10 MPa), or largest volume (14.14 km³). Oblate sources produce the greatest displacement difference magnitudes, prolate shaped typically producing the smallest, with depth variance producing the largest uplift differences across all three source shapes.

Shallow pressure sources with volumes less than 4.19 km³, depths greater than 5 km, and overpressures less than 6 MPa, across all three tested source shapes, fail to generate displacement difference values above the threshold mark of 10 mm. This failure indicates that in stacked magmatic systems, displacements from the deeper, larger storage reservoir can hide any deformation caused by the shallower reservoir. False analyses of magmatic storage regions beneath a volcanic edifice can lead to inaccurate interpretations of volcanic deformation episodes, having potential impacts on future eruption forecasting and hazard assessment efforts.

Maximum vertical displacement differences, excluding prolate shaped sources, are observed directly above the pressure source. Models constructed here assume a pseudo-3D geometry using vertically stacked cavities to mimic magmatic storage reservoirs. However, horizontal offsets between shallow and deep reservoirs, a common feature in volcanic systems, should produce different displacement difference patterns as the footprint above the pressure sources is no longer shared. Horizontally offsetting storage reservoirs however is only possible using 3D model environments. Modelling how individual parameters alter surface displacements within a 2D model space can benchmark future studies using 3D geometries and more realistic volcanic systems.

Chapter 4:
**Multiple Pressure Source Numerical
Deformation Modelling of the
Sakurajima Volcano and Aira Caldera
Magmatic System**

Abstract

Sakurajima volcano, the active vent of Aira caldera, is one of the most active volcanoes in Japan. Long term surface inflation, together with almost daily Vulcanian eruptive activity, highlights the risk of a potentially larger eruption. To aid eruption forecasting and hazard assessments, a greater understanding of the magmatic system beneath the volcano is required. Here, deformation patterns around the volcano between 1996 – 2007 have been re-examined to constrain the location and parameters of a potential shallow magma storage region beneath the Sakurajima volcanic edifice. Previous analytical studies of Aira caldera assumed an unrealistic homogeneous crust, potentially impacting pressure source location and magnitude estimates. Finite Element modelling was conducted, incorporating subsurface heterogeneities and surface topography. Gravity modelling was then undertaken using the most likely magmatic system arrangement, to compare with measured gravity data to further constrain the magma system model.

Results show a double source magmatic system better represents the measured deformation than a single source at a depth of 13 km in the northeast of Aira caldera. The best fit shallow secondary source is prolate shaped, at a depth of 7 km, located towards the northwest of the active Minamidake vent. This optimal shallow source contrasts with previous analytical estimates, highlighting the effects of incorporating crustal heterogeneity. Gravity modelling suggests the optimal location is north of the Minamidake vent, however strong limitations are present due to poor resolutions with the inferred subsurface density distributions. Future deformation and gravity modelling of the Aira caldera magmatic system will benefit from the inclusion of higher resolution geophysical imaging data, improving interpretations of surface deformation leading up to eruptions, with similar methods being applicable to volcanoes world-wide.

4.1 Introduction

Accumulation and migration of magma causes a transfer of stress and strain through the Earth's crust, often deforming the surface [*Gudmundsson*, 2012; *Acocella*, 2021]. Surface deformation produced by a magmatic system can aid in with eruption forecasting and hazard assessment by providing a means to locate and assess the magnitude of magma storage at depth [*Poland et al.*, 2006; *Parks*

et al., 2012; *Fernández et al.*, 2017], with first order estimates made possible by simple analytical models [e.g., *Mogi*, 1958; *McTigue*, 1987; *Fialko et al.*, 2001]. However, first order estimates are not always sufficient in volcanic settings where higher levels of accuracy are required, such as in response to volcanic activity in a high-risk area, or in preparation for future activity. The inclusion of topography, and seismic geophysical imaging, can produce significant differences in modelled deformation patterns, improving estimates of the conditions of the magma supply and storage in a volcanic system [*Hickey et al.*, 2016; *Acocella*, 2021]. Numerical modelling techniques, such as the Finite Element Method, possess the capacity to incorporate different subsurface mechanical properties, rheologies, and geometries [*Masterlark*, 2007; *Del Negro et al.*, 2009; *Gregg et al.*, 2012; *Bonaccorso et al.*, 2013; *Currenti*, 2014]. Despite producing a better representation of subsurface mechanical conditions [e.g., *Hickey et al.*, 2016], the inclusion of extra parameters, such as subsurface heterogeneity, is not commonly applied in geodetic modelling. This limitation highlights deficiencies in some current approaches to geodetic modelling, showing potential paths for an improved understanding of subsurface processes driving surface deformation, leading to better eruption forecasting and hazard assessments.

At the southern end of the Island of Kyushu, lies Aira Caldera (Figure 4.1). This feature, one of a series of calderas located within the NNE-SSW Kagoshima graben, was formed by a VEI 7 Plinian eruption 29,000 years ago [*Aramaki*, 1984; *Okuno*, 2002]. Today the 17 km by 23 km caldera mostly lies within Kagoshima Bay. On Aira caldera's southern rim lies Sakurajima, Japan's most active volcano. Eruptions have occurred almost daily at Sakurajima since 1955, specifically from the southern of the two main vents, Minamidake, and a parasitic vent 500 m to the east, Showa Crater [*Hotta et al.*, 2016]. Three main major eruptive events have occurred within the historical past, the last of these, the 1914 VEI 4 "Taisho" eruption, led to the deaths of 58 people [*Yamaguchi*, 1975]. Given the eruptive present and destructive past of the volcano, Sakurajima is under 24-hour surveillance to protect the 600,000 citizens of Kagoshima City (8 km west), as well as the 5,000 on the volcano itself [*Hickey et al.*, 2016].

Sakurajima has a long history of recorded deformation, with levelling data stretching back to 1892 [*Omori*, 1916], supplemented by additional data following the start of the long standing eruptive episode of the volcano in 1955 (Figure 4.2)

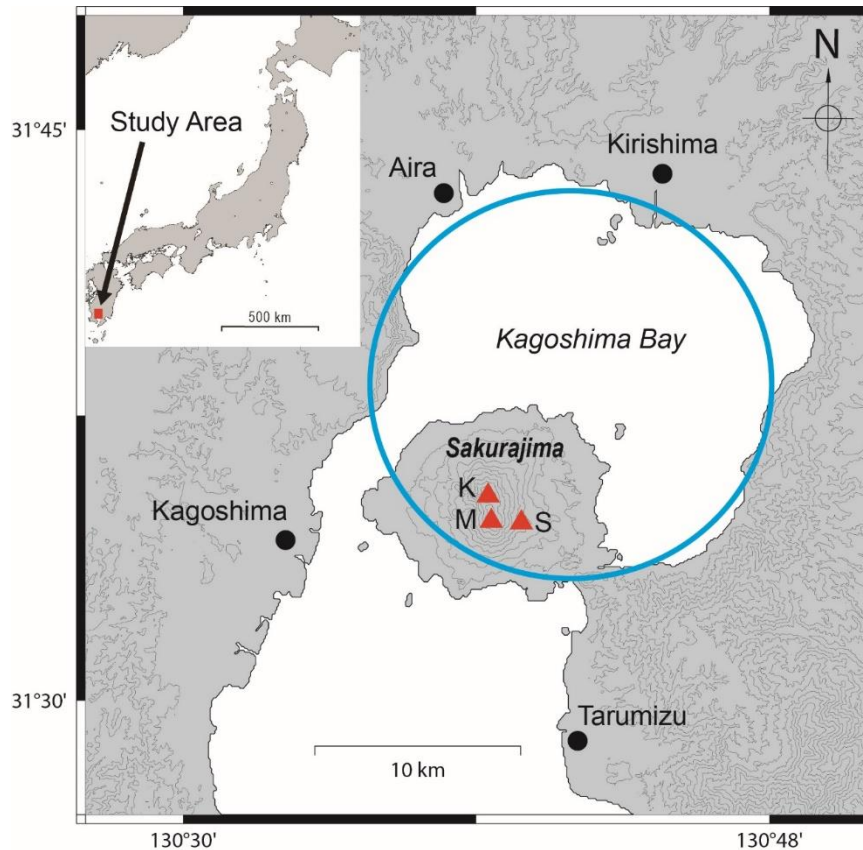


Figure 4.1: The geography of Kagoshima Bay. The blue circle shows the extent of Aira caldera, with red triangles the peaks and main vents of the volcano: K = Kitadake, M = Minamidake, and S = Showa crater.

[Hotta *et al.*, 2016]. Concentric ground subsidence around Aira Caldera due to the 1914 Taisho event [Omori, 1916], and numerous further episodes of deformation since 1955, have been used to produce estimates of the location of potential pressure sources within the magmatic system. Results from analytical modelling suggest a major source 8 – 11 km below Aira Caldera [Mogi, 1958; Eto, 1989; Iguchi *et al.*, 2008; Iguchi, 2013], and a shallower minor source (3 – 6 km) beneath Sakurajima [Yokoyama *et al.*, 1986; Eto, 1989; Iguchi, 2013; Hotta *et al.*, 2016]. Despite an extensive history of geodetic modelling of Aira caldera and Sakurajima volcano, most studies have been conducted using the analytical elastic half-space and spherical source principles pioneered by Mogi [1958]. The failure to account for subsurface variability in material properties within the Earth's crust, as well as a wider range of potential source geometries and configurations, mean estimates of pressure source characteristics within the magmatic system could be improved.

Numerical modelling techniques have the capacity to reduce the limitations of

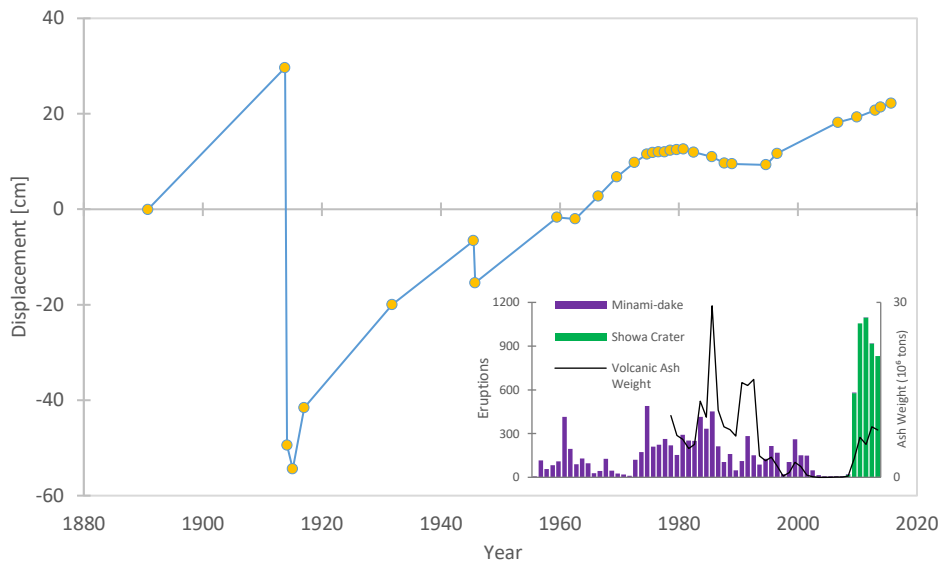


Figure 4.2: Deformation history of Aira caldera, and recent eruptive history of Sakurajima. Levelling benchmarks are shown as yellow dots on the main figure. The inset figure shows eruption frequencies from main eruptive vents since 1955 (Miniamidake and Showa Crater), and accompanying volcanic ash weights since 1978. Adapted from Hickey et al. [2016].

analytical methods by accounting for additional realistic complexities, including a heterogenous crust, topography, and crustal rheologies other than linear elastic, amongst others [Masterlark, 2007; Del Negro et al., 2009; Bonaccorso et al., 2013; Currenti et al., 2014]. However, only one numerical study has been conducted at Sakurajima, and despite the consensus that the magmatic system hosts multiple pressure sources, the study used only one pressure source [Hickey et al., 2016]. Using deformation data over the same time period (1996 – 2007) as a previous analytical study [Iguchi et al., 2008], Hickey et al. [2016] found that notable differences in the depth, shape, and location, were present between the best fit pressure source solutions (Table 4.1), highlighting the impact of differences between each of the methods. Despite improving the overall fit to the deformation data, whilst accounting for more model complexity, prominent misfits remained in the numerical (Finite Element) study, and which Hickey et al. [2016] suggested could be caused by a dyke connecting the Aira source and Sakurajima vent that had not been included in their model. A shallow source beneath Sakurajima was not mentioned to account for misfits, but remains a possibility given its prominence in analytical modelling results [Yokoyama et al., 1986; Eto, 1989; Iguchi, 2013; Hotta et al., 2016].

	<i>Iguchi et al., 2008</i>	<i>Hickey et al., 2016</i>
Longitude (°)	130° 41' 16.80"	130° 44' 31.20"
Latitude (°)	31° 38' 27.60"	31° 39' 50.40"
Depth (km)	11	13
Shape	Spherical	Oblate

Table 4.1: Best fit pressure source parameters for analytical [*Iguchi et al., 2008*] and numerical [*Hickey et al., 2016*] studies of the 1996 – 2007 deformation period at Aira caldera.

Discerning between similar deformation profiles caused by different source geometries or natures (e.g., magmatic, hydrothermal, or hybrid) can be achieved by microgravity modelling [*Battaglia et al., 2009; Fernández et al., 2017*]. The movement of masses within the subsurface, such as magma migration, causes changes in the subsurface density distribution, altering the Bouguer anomaly around a volcanic edifice [*Gottsmann et al., 2002; Dzurisin, 2003*]. Finite Element microgravity modelling has been used in volcanic settings [*Currenti et al., 2007; Gottsmann, Biggs, et al., 2020*], with predicted deformations commonly calculated alongside gravity changes. Bouguer anomalies can be used to infer coordinates, natures, and depths of combined mass changes and pressure sources, helping to improve the accuracy of purely deformation focused modelling efforts [*Currenti et al., 2007; Battaglia et al., 2008; Fernández et al., 2017*].

This study used deformation data from Aira caldera between 1996 – 2007 to conduct the first numerical study of Aira caldera and Sakurajima volcano, assuming a multiple pressure source magmatic system. Varying coordinates, depth, size, and shape, of a potential secondary shallow pressure source beneath the Sakurajima volcanic edifice were tested using finite element modelling to assess whether a multiple pressure source system better represents the measured observed deformation than a single source results, the later assumed in previous studies [*Iguchi et al., 2008; Hickey et al., 2016*]. Modelling of the resultant Bouguer anomalies of the potential best fit deformation solutions then helped to provide an optimal arrangement for the magmatic system.

4.2 Methods

4.2.1 Datasets

Deformation

Continuous GPS records from the 1996 – 2007 period were used, with both vertical and horizontal components (Figure 4.3) [Iguchi *et al.*, 2008; Hickey *et al.*, 2016]. Deformation highlights a radial outward expansion emanating from Aira caldera. Sakurajima was uplifted by 12 cm over the 11 years of data collection, with the maximum level of vertical displacement observed at FUTG station.

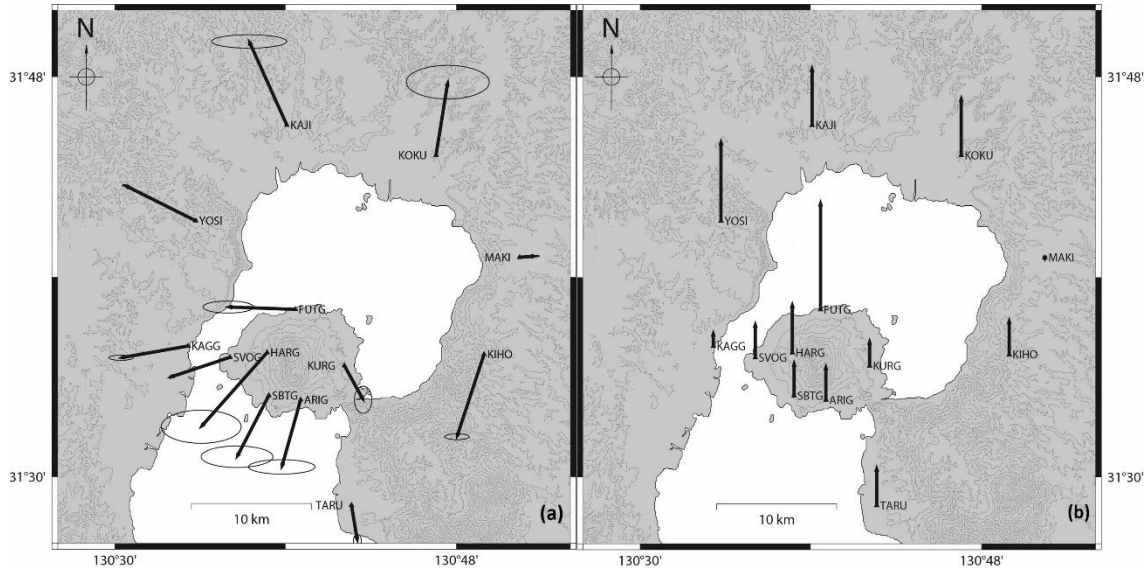


Figure 4.3: Measured GPS deformation at Aira caldera from 1996 – 2007. Horizontal (a) and vertical (b) displacements are shown, along with the names and locations of GPS stations. Ellipses on (a) represent error estimates of the instruments used to measure displacements. The maximum and minimum displacements are 8.24 cm and 1.30 cm horizontally (HARG and MAKI stations) and 15.9 cm and -0.2 cm vertically (FUTG and MAKI stations).

Gravity

Bouguer gravity anomaly data was used from the Geological Survey of Japan and Gravity Research Group in Southwest Japan [Komazawa *et al.*, 2000; Shichi, 2001], supplemented with additional data from the Kagoshima district and Sakurajima volcano areas [Miyamachi *et al.*, 2000; Murata *et al.*, 2007; Komazawa *et al.*, 2008]. In total, 2,754 individual data points from across the Kagoshima area were used, and were acquired individually using static gravimeter measurements during each successive survey. The data used was collected between 1975 and 2007. The Bouguer anomaly distribution from around Kagoshima Bay shows a large negative anomaly at its center, with the lowest value around -25 mGal (Figure 4.4). Over Sakurajima volcano, a smaller, isolated anomaly exists of -10 mGal beneath the Kitadake peak, with lower values visible along the length of the Kagoshima graben.

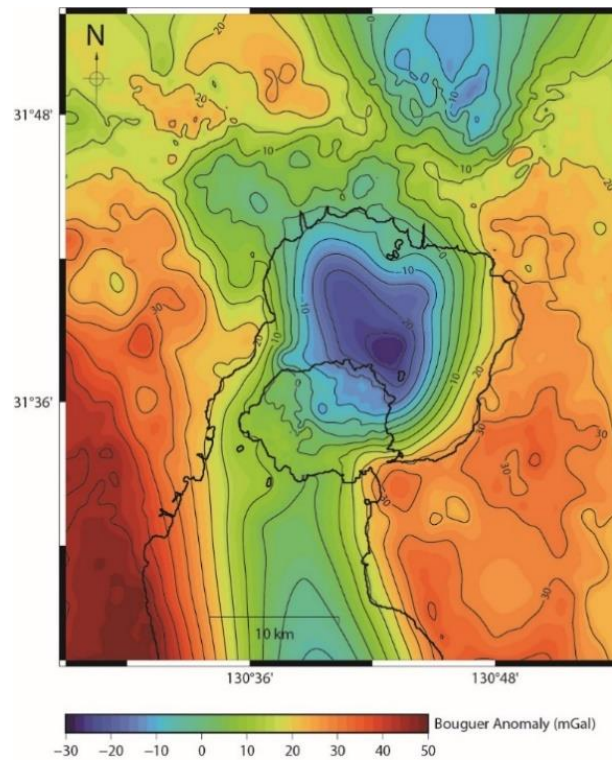


Figure 4.4: Measured Bouguer anomaly distribution across Kagoshima Bay. The alignment of the Kagoshima graben can be seen by the NNE-SSW trend of negative values.

4.2.2 Deformation Model Setup

Construction and computation of all models in this study used the Finite Element software COMSOL Multiphysics (v5.5).

Geometry

Models were constructed using a full 3D geometry, by incorporating the topography, bathymetry, and subsurface seismic tomography data of the Kagoshima Bay area [Alanis *et al.*, 2012; Hickey *et al.*, 2016]. The shallow pressure source was modelled as either a pressurized oblate, prolate, or spherical cavity. The deep pressure source was an oblate shaped cavity throughout every model iteration [Hickey *et al.*, 2016]. Surrounding the model geometry was an Infinite Element Domain (IED) to assist in limiting boundary effects in the interior of the model [Hickey *et al.*, 2014]. The final model had dimensions of 88 km x 88 km x 30 km, containing an average of 420,000 mesh elements, with higher mesh resolution around the GPS site locations and each pressure source. Boundary conditions for the model were adapted from Hickey *et al.* [2014], using the same process of application to a 3D geometry as Hickey *et al.* [2016]. A free top and fixed bottom constrain the vertical elements of the

model, with horizontal components contained by lateral rollers and 2 km thick IED (Figure 4.5a). Finally, a boundary load was assigned normal to the surface of the sources to simulate the effects of an overpressure on the surrounding crust (Figure 4.5b).

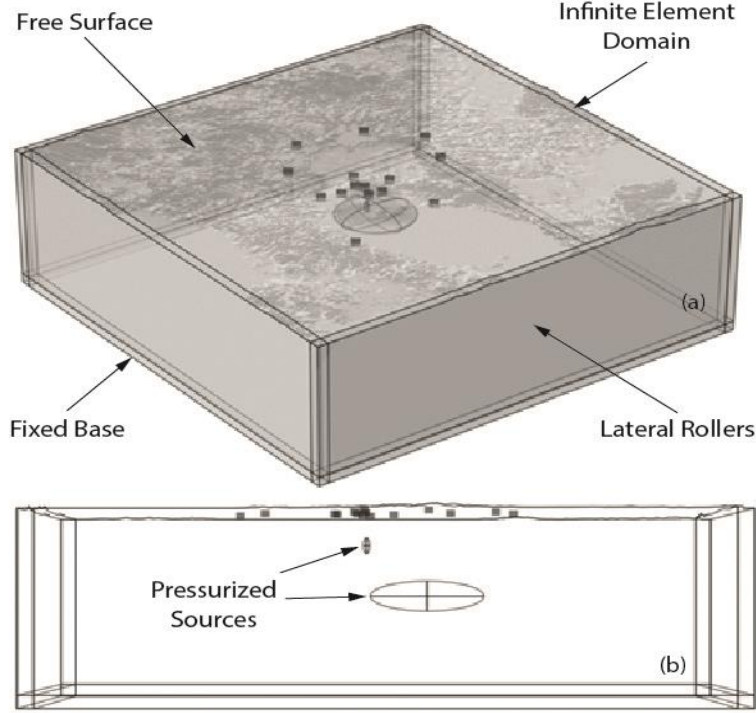


Figure 4.5: Finite Element model for Aira caldera. (a) Boundary conditions and model geometry. (b) Arrangement of the pressurized sources, modelled as cavities for this study.

Material Properties

The 3D subsurface heterogeneity in material properties was inferred from seismic tomography data beneath Aira caldera [Alanis *et al.*, 2012; Hickey *et al.*, 2016]. Seismic velocities V_p and V_s were converted to calculate crustal values of density, ρ , Young's Modulus, YM, and Poisson's Ratio, ν , using the following set of equations [Brocher, 2005]:

$$\nu = 0.5 \times \left[\left(\frac{V_p^2}{V_s^2} \right) - 2 \right] / \left[\left(\frac{V_p^2}{V_s^2} \right) - 1 \right] \quad (4.1)$$

$$\rho = 1.6612V_p - 0.4721V_p^2 + 0.067V_p^3 - 0.0043V_p^4 + 0.000106V_p^5 \quad (4.2)$$

$$YM = \frac{V_p^2 \rho (1 + \nu)(1 - 2\nu)}{(1 - \nu)} \quad (4.3)$$

Young's Modulus and Poisson's ratio values used varied from 30 – 50 GPa and 0.2 – 0.25 at the surface, to between 50 – 80 GPa and 0.25 – 0.28 at 30 km below sea level. All model iterations use an elastic rheology throughout to focus the modelling on spatial deformation patterns rather than time-dependent phenomena, hence viscoelastic rheologies were not considered during this study.

4.2.3 Deformation Modelling Approach

The parameters used for the main deep pressure source beneath Aira caldera were the best fit solutions from *Hickey et al* [2016]; an oblate shaped (semi-major axis = 2.4 km, semi-minor axis = 7.2 km) reservoir, located at a depth of ~13 km beneath the north-eastern section of the caldera (X = 130° 44' 31.20", Y = 31° 39' 50.40"), with an over-pressure of 2.7 MPa. These deep source parameters were kept constant throughout every model iteration.

For deformation modelling, a total of 18 coordinate sets were used. The longitude and latitude of search coordinates for the shallow pressure source were determined using a 4 x 4 grid, with each point being around 1 km apart, covering an area of roughly 9.2 km² around the Minamidake vent (Figure 4.6). Two additional sets of coordinates were also considered: Minamidake vent (X = 130° 39' 32.43", Y = 31° 34' 46.24"), which is the inferred location from the analytical studies [*Eto*, 1989; *Iguchi*, 2013; *Yamamoto et al.*, 2013], and the small -10 mGal anomaly in the measured Bouguer distribution 1.7 km north of Minamidake (X = 130° 39' 36.60", Y = 31° 35' 39.49"), as a negative anomaly is indicative of density deviations below that section of the edifice.

The coverage of the search grid was confined to an area surrounding the eruptive vents and edifice. The grid was selected to cover an assumed geologically realistic area around the eruptive vents in which a potential shallow storage region within the magmatic system could exist [*Ebmeier et al.*, 2018]. Overpressures, depths, and volumes of the secondary shallow source were varied from 10 MPa – 50 MPa, 3 km – 7 km, and 0.004 km³ – 0.524 km³, respectively (Table 4.2). Spheroids of different eccentricities were tested, with oblate, spherical, and prolate shapes used: dipping sources however were not considered. To isolate and compare displacement patterns for the different source shapes, the volumes of the prolate and oblate sources were set to equal the equivalent spherical source, with the length of each axis calculated using a

set ratio (1:3, 1:2, 1:1, 2:1 and 3:1) between the semi-major and semi-minor axes (Table 4.3).

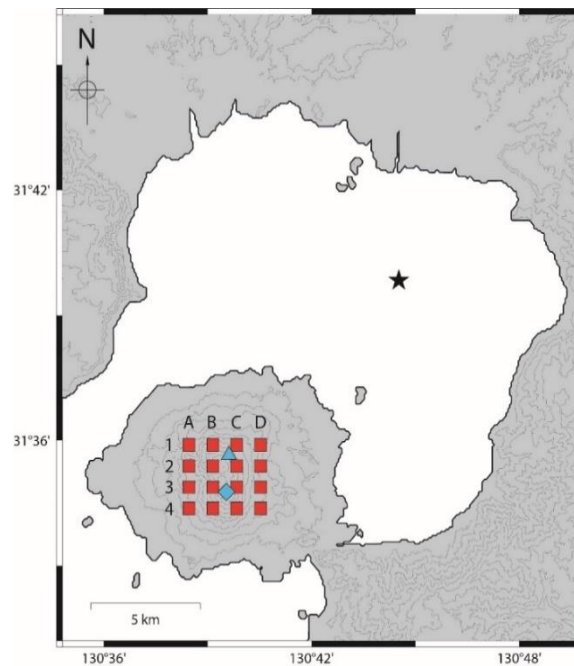


Figure 4.7: Grid coordinates. Tested coordinates of the shallow minor pressure sources (red squares), alongside the major reservoir from Hickey et al [2016] (black star). Range of shallow coordinates used are simplified to $X = A - D$ and $Y = 1 - 4$. The blue triangle and diamond show the locations of the -10 mGal anomaly and Minamidake vent.

Shapes	Overpressures (MPa)	Volume (km ³)	Depths (km)
Spherical	10	0.004	3
Oblate	30	0.113	5
Prolate	50	0.524	7

Table 4.2: Full range of shallow source parameters tested.

	R (km)	Semi-Major (km)	Semi-Minor (km)	Volume (km ³)
Spherical	0.1	-	-	0.004
	0.3	-	-	0.113
	0.5	-	-	0.524
Oblate 1:2	-	0.126	0.063	0.004
	-	0.378	0.189	0.113
	-	0.630	0.315	0.524
Oblate 1:3	-	0.144	0.048	0.004
	-	0.433	0.144	0.113
	-	0.721	0.240	0.524
Prolate 2:1	-	0.079	0.159	0.004
	-	0.238	0.476	0.113
	-	0.397	0.794	0.524
Prolate 3:1	-	0.069	0.208	0.004
	-	0.208	0.624	0.113
	-	0.347	1.040	0.524

Table 4.3: Tested range of source shapes and sizes.

The fit of each individual magmatic source arrangement was calculated using an error weighted misfit function, F , between measured and predicted surface displacements, using the following equations:

$$W_i = \frac{\left| \frac{D_i}{E_i} \right|}{\sum \left| \frac{D_i}{E_i} \right|} \quad (4.4)$$

$$f_i = [W_i(M_i - D_i)]^2 \quad (4.5)$$

$$F = \sqrt{\sum f_i} + 1 \quad (4.6)$$

The variables D , E , M , and W represent the data, error, model, and weight values across the full range of stations in the GPS network for each GPS displacement vector. The optimal misfit value of 1.003113 from *Hickey et al.* [2016] was used as a benchmark, allowing for direct comparisons with the resulting misfit value from each possible shallow source iteration, with lower values representing a better fit to the measured deformation data from the investigated period.

Preferred source shape was established first by constructing a shallow pressure source at each of the 16 grid coordinates using all three source shapes. To limit computation time, only the median values for overpressure (30 MPa), volume (0.113 km), or depth (5 km) (Table 4.2) were used for these tests, totalling 80 different combinations. The shape producing the lowest misfit values was then selected. Once the optimal source shape was determined, shallow pressure sources of the optimal shape were tested at each of the 18 possible coordinates using the full range of the remaining parameters (depth, pressure, volume), with a total of 484 combinations (432 from the grid, 52 from the Minamidake and -10 mGal anomaly coordinates). The combination with the lowest misfit, provided that the value was also less than the *Hickey et al.* [2016] threshold, was used to represent the optimal solution in the deformation modelling.

4.2.4 Gravity Modelling

An additional level of scrutiny was applied by modelling the resultant surface gravity anomaly produced by a selection of pressure source solutions, to compare with measured gravity data from Kagoshima Bay. Three sets of shallow source

coordinates were used: the best fit coordinates from the deformation modelling, Minamidake vent ($X = 130^{\circ} 39' 32.43''$, $Y = 31^{\circ} 34' 46.24''$), and the small -10 mGal anomaly observed 1.7 km north of Minamidake ($X = 130^{\circ} 39' 36.60''$, $Y = 31^{\circ} 35' 39.49''$). The same deep source assumed in the deformation modelling ($X = 130^{\circ} 44' 31.20''$, $Y = 31^{\circ} 39' 50.40''$, $Z = 13$ km, semi-major axis = 2.4 km, semi-minor axis = 7.2 km) was used for each of the three coordinate sets.

The following Poisson's differential equation was used to extract the vertical component of the gravitational potential ϕ_g [Cai *et al.*, 2005; Currenti *et al.*, 2007], which incorporated a density distribution derived from subsurface seismic tomography data (Equation 4.2):

$$\nabla^2 \phi_g = -4\pi G \Delta\rho(x, y, z) \quad (4.7)$$

where G is the universal gravitational constant ($6.674 \times 10^{-11} \text{m}^3 \text{kg}^{-1} \text{s}^{-2}$), and $\Delta\rho(x, y, z)$ is the change in density across the 3D model domain.

The three shallow sources tested were all assumed to possess the same shape, depth, and size as the best fit pressure source, with coordinates being the only differentiating factor; boundary loads (overpressures) were no longer required and the sources were modelled here using physical properties (i.e., a density) rather than cavities. To account for low spatial resolution of the inferred subsurface density values, estimations of the density contrast between the material of the pressure sources and the immediately adjacent crust were made with values between $0 - 500 \text{ kg/m}^3$ at 100 kg/m^3 intervals for both the shallow and deep sources: the average density contrast between crustal rock (2750 kg/m^3) and magma (2400 kg/m^3) is around 350 kg/m^3 [Acocella, 2021]. We do not account for potential gravity changes caused by deformation as both models were conducted independently of each other as a first-order investigation.

Six density contrasts were applied to each of the three shallow coordinates sets, giving a total of 18 combinations. The modelled Bouguer anomaly distributions from the coordinate sets and density contrast combinations were compared with the gravity distribution from Kagoshima Bay, using the same misfit analysis as the deformation modelling. The coordinate set and density contrast arrangement with the lowest misfit represented the optimal solution for the gravity modelling.

4.3 Results

4.3.1 Shallow Pressure Sources

Source Shape

Five different spheroidal eccentricities were evaluated for the shallow pressure source, to determine an optimal shape going forward for the rest of the modelling process. Overall, a shallow prolate source with a 3:1 axis ratio produces the best fit to the measured data across all three parameter searches, with double pressure source models with a prolate shallow source producing lower misfits than a single source (Figure 4.7). An oblate source with a 1:3 axis ratio consistently produced the worst fit to the data, often resulting in double source arrangements with higher misfits than a single source.

Optimal Parameters

Using the prolate source determined from the source shape analysis, the full parameter ranges of overpressure, depth, and size were applied to the 4 x 4 grid of possible X-Y coordinates for a shallow source beneath Sakurajima, as well as the gravity low and Minamidake vent coordinates. The resultant misfit between modelled and measured data was used to assess each model iteration for an optimal set of parameters.

Of the 484 double source combinations tested, 188 combinations (38.84%) generated misfits lower than the single source model, with 167 from the search grid (Figure 4.8). All 18 sets of coordinates produce at least 1 misfit value below the single source threshold. From the grid search, each of the three depths and overpressures produced sub-threshold misfits, with a depth of 7 km (53.29%) and an overpressure of 10 MPa (46.11%) being the most common amongst sub-threshold shallow source combinations. The most frequent volume amongst sub-threshold shallow source arrangements was 0.113 km³ (66.47%), and the smallest volume (0.004 km³) was the only parameter not to have any arrangements with a sub-threshold data fit.

Isolating the 10 lowest misfit values shows significant preferences toward certain parameters (Table 4.5). Westward longitude values dominate, with the top 8 combinations all possessing the most western value of 130° 38' 27.55" (A1,

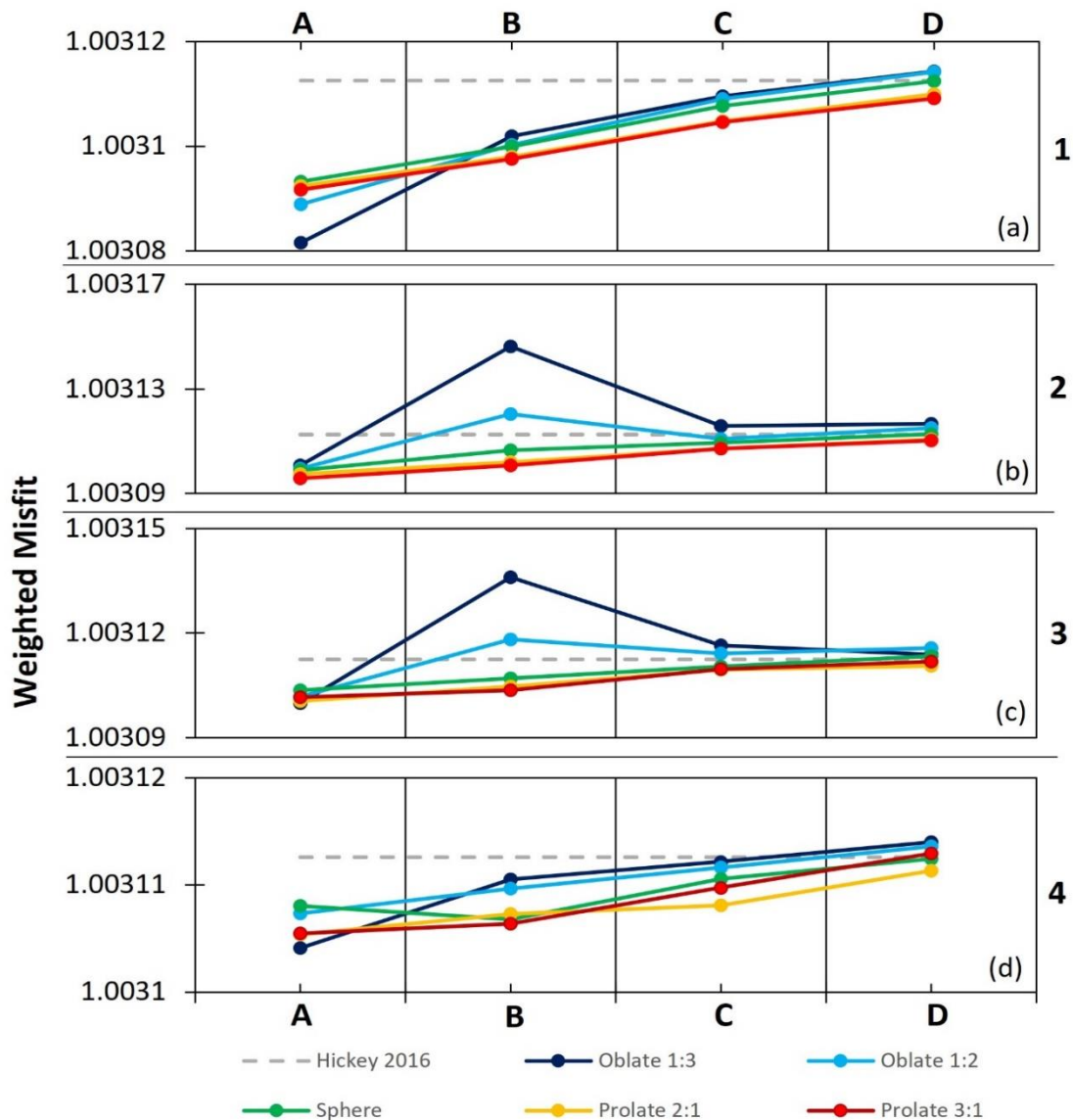


Figure 4.9: Source shape parameter sensitivity test misfit values, resulting from 5 different shallow pressure sources used at each of the 16 grid coordinates (Figure 6). The grid latitude coordinates 1 (a), 2 (b), 3 (c), and 4 (d) are displayed vertically to show how each shape misfit changes across the longitude values A, B, C, and D. The *Hickey et al.* [2016] threshold value is displayed as a horizontal dotted grey line.

Figure 4.6); latitudes show an even split across all 4 possible values. Only the maximum depths (7 km) and volumes (0.524 km^3) are present, with pressures split between 30 and 50 MPa; the top 4 values possess the maximum overpressure of 50 MPa. Similarly, both Minamidake vent and the -10 mGal anomaly produce their lowest misfit values with depths and volumes at 7 km and 0.524 km^3 respectively, with an optimum overpressure of 30 MPa. The lowest misfits from these two additional coordinates however are greater than those present in the top 10 from the 4 x 4 search grid.

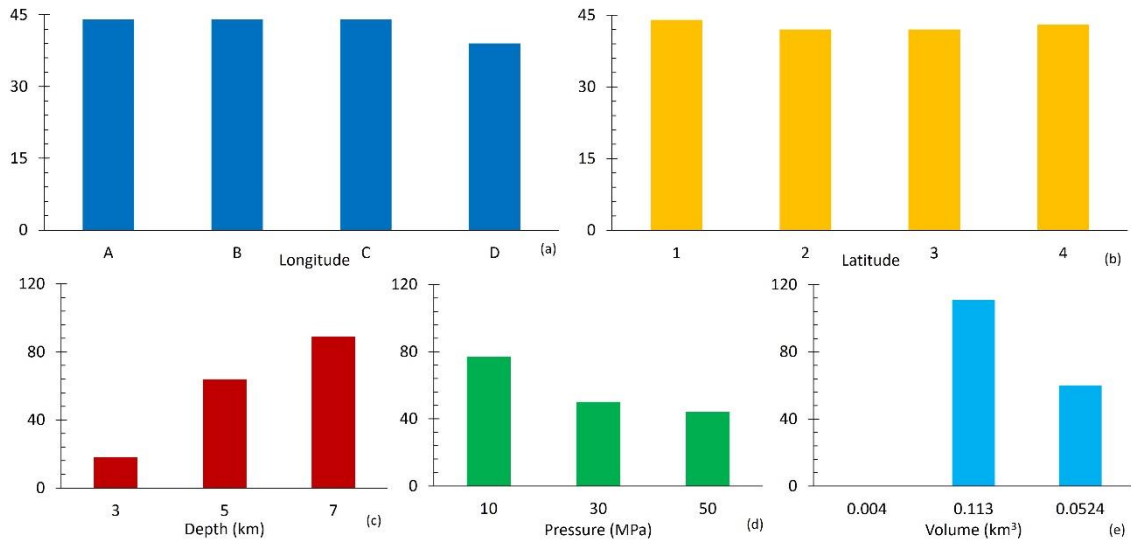


Figure 4.10: Frequency of best fit parameters. Occurrences of (a) longitude, (b) latitude, (c) depth, (d) pressure, (e) volume from the 167 double source combinations that produce misfits below the single source threshold value from the search grid.

<i>F</i>	<i>X</i>	<i>Y</i>	<i>Depth (km)</i>	<i>Pressure (MPa)</i>	<i>Volume (km³)</i>
1.003043	A	1	7	50	0.524
1.003049	A	2	7	50	0.524
1.003054	A	3	7	50	0.524
1.003058	A	4	7	50	0.524
1.003058	A	1	7	30	0.524
1.003062	A	2	7	30	0.524
1.003065	A	3	7	30	0.524
1.003067	A	4	7	30	0.524
1.003072	B	1	7	30	0.524
1.003075	B	2	7	30	0.524
1.003081	-10 mGal Anomaly		7	30	0.524
1.003089	Minamidake Vent		7	30	0.524

Table 4.4: Top 10 grid search parameter arrangements. Lowest misfit values observed in the 167 double source arrangement with lower misfits than a single source. The bottom two values are the lowest misfit solutions from the -10 mGal anomaly and Minamidake vent respectively.

The lowest misfit value observed in all grid searches is located 2.8 km northwest of the Minamidake vent ($X = 130^{\circ} 38' 27.55''$, $Y = 31^{\circ} 35' 53.89''$, grid coordinate A1) at a depth of 7 km, with a reservoir overpressure of 50 MPa, and a volume of 0.524 km^3 (semi-major axis = 0.347 km, semi-minor axis = 1.040 km) (Figure 4.9). Overall, the deformation modelling results show that the addition of a small, shallow source to the magmatic system does produce a better data-fit than a single deep source beneath Aira caldera.

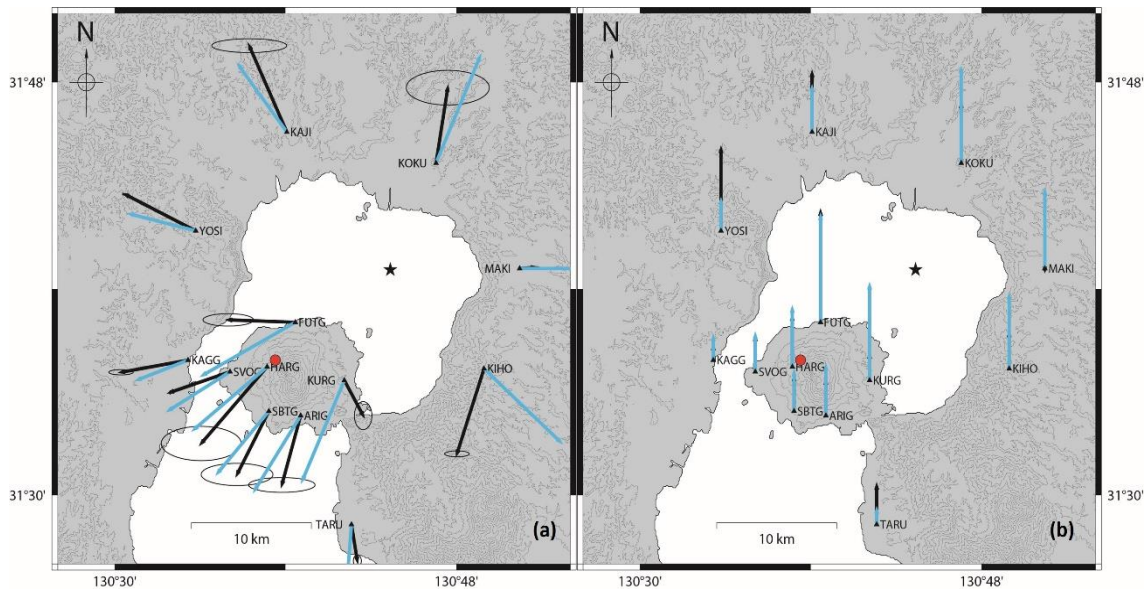


Figure 4.11: Modelled best fit deformation vectors. Black lines show deformation from the measurement period of 1996 - 2007, with blue arrows showing the best fit modelled horizontal (a) and vertical (b) displacements. The red circle and black star show the locations of the shallow and deep pressure sources used. The maximum and minimum displacements are 9.52 cm and 1.02 cm horizontally (KOKU and HIRA stations) and 15.3 cm and 0.24 cm vertically (FUTG and HIRA stations).

4.3.2 Bouguer Anomaly Distributions

The best fit deformation shallow source ($X = 130^{\circ} 38' 27.55''$, $Y = 31^{\circ} 35' 53.89''$, $Z = 7$ km, semi-major axis = 0.347 km, semi-minor axis = 1.040 km, $\Delta P = 50$ MPa) was used in gravity modelling, along with the coordinates of the Minamidake vent ($X = 130^{\circ} 39' 32.43''$, $Y = 31^{\circ} 34' 46.24''$), and the observed -10 mGal anomaly 1.7 km north of Minamidake ($X = 130^{\circ} 39' 36.60''$, $Y = 31^{\circ} 35' 39.49''$). Depths (7 km) and volumes (0.524 km^3) were kept constant for each of the three coordinate sets as these produced the lowest misfit values during the deformation modelling.

Analysis of the range of density contrasts applied to both pressure sources show the largest density contrast (500 kg/m^3) produces the lowest misfits across all three coordinates used, with the smallest density contrast (0 kg/m^3) producing the highest misfits. For each of the three coordinates used, the increase of density contrast improves fit to the gravity data (Figure 4.10); at the density contrast producing the best data fit (500 kg/m^3), all three coordinates produce similar misfit values. The lowest misfit values of 871.29 (Gravity Anomaly), 871.32 (Deformation Best Fit) and 871.39 (Minamidake), highlight how marginal the

difference is between these three coordinate sets.

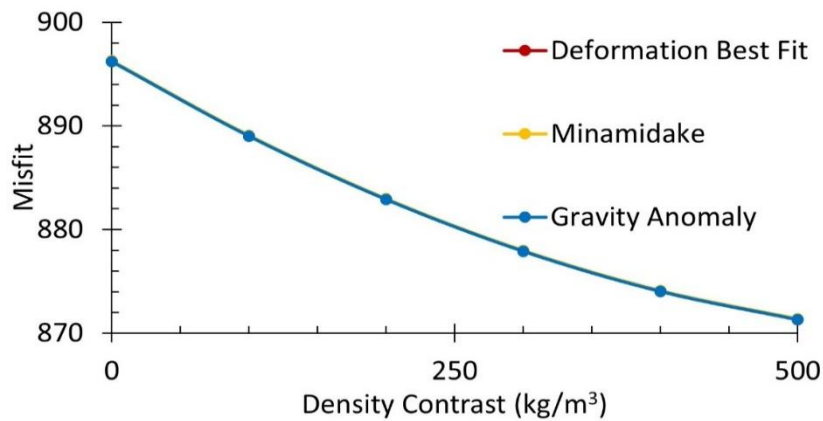


Figure 4.12: Gravity modelling comparisons between observed and simulated data for the three gravity source coordinates tested and the density contrast between the sources and the surrounding crustal domains. The results are essentially indistinguishable from one another, with the red and yellow lines obscured by the blue line.

The resultant modelled Bouguer anomaly distributions from the magmatic source arrangements produce poor fits to the Bouguer data for all three examples (Figure 4.11), with high levels of misfit at Kagoshima Bay and the northern flank of Sakurajima volcano. The distinctive large -30 mGal anomaly seen in the gravity data in the north-eastern section of Kagoshima Bay is not present, although modelled results do show a region of lower gravity of around 0 mGal in the same area. Southwestern portions of Sakurajima volcano and Kagoshima City, however, more closely resemble the measured data.

4.4 Discussion

4.4.1 Shallow Source Location

Seismic data suggests a shallow reservoir 3 – 6 km beneath Sakurajima [Iguchi, 2013], which is supported by analytical deformation modelling [Yokoyama *et al.*, 1986; Eto, 1989; Iguchi, 2013; Hotta *et al.*, 2016]. The depth of the best fit deformation model from this study (6 – 8 km) supports both the previous seismic and analytical shallow storage estimates, since the shallow prolate source extends into the 3 – 6 km depth region. However, since the shallow pressure source is 2.8 km northwest of Minamidake, it suggests a lateral offset between source and vent, contrasting with the analytical estimates of the shallow magmatic system, which place secondary sources directly beneath the active vent of Minamidake. Magmatic systems can be considered as laterally extensive,

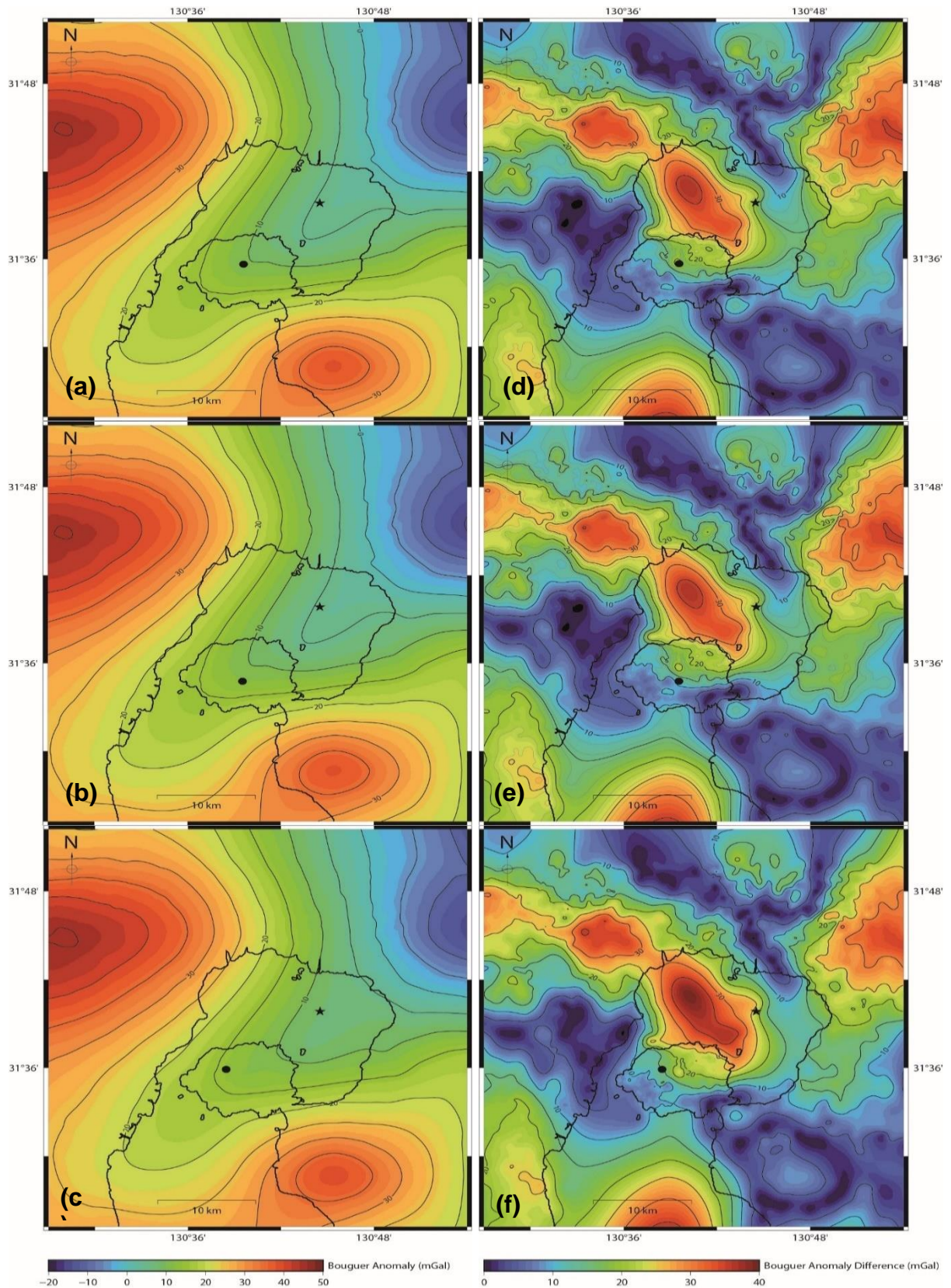


Figure 4.14: Modelled Bouguer anomalies and misfits. Modelled gravity fields (a – c) and the difference between the modelled and observed anomalies (d – f) for the -10 mGal anomaly (a & d), Minamidake Vent (b & e), and the best fit deformation coordinates (c & f). The black stars and circles represent the locations for the deep and shallow pressure source for each arrangement.

with offsets of <5 km between source and vent being common in other volcanic systems around the world [Ebmeier *et al.*, 2018]. The change in lateral location between the numerically estimated shallow source, and those estimated using analytical techniques, could be driven by the inclusion of subsurface heterogeneity [Masterlark, 2007; Del Negro *et al.*, 2009; Bonaccorso *et al.*, 2013; Currenti *et al.*, 2014; Hickey *et al.*, 2016; Cabaniss *et al.*, 2020].

From petrological and geochemical studies, mainly through the diversity in erupted lava compositions, the Aira magmatic system is hypothesised to contain multiple dacitic magma chambers [Shibata *et al.*, 2013], or a trans-crustal magmatic system (TCMS) [Zawalna-Geer *et al.*, 2019; Brown *et al.*, 2020]. A TCMS differs from the traditional view of a melt dominated magma chamber, in that it consists of a crustal-scale column of crystal mush, containing varying proportions of silicate melt, with dispersed pockets of magma [Cashman *et al.*, 2017; Hammond *et al.*, 2019; Svoboda *et al.*, 2021]. The petrological evidence for the presence of a multitude of shallow storage reservoirs implies that different regions could supply magma during separate deformation periods.

Upward emplacement of magma from shallow reservoirs would also likely be accompanied by volcano-tectonic (VT) earthquakes. The majority of VT hypocentres, especially in the last 10 years, are located directly beneath Minamidake vent, representative of the current active state of the volcano [Hidayati *et al.*, 2007; Iguchi, 2013; Hickey *et al.*, 2016]. However, only isolated events occurred at the best fit deformation location 2.8 km northwest of Minamidake. This lack of VT hypocentres around the hypothesised shallow pressure source region may suggest that inflation occurred aseismically. Deformation in ductile materials can occur without visible fracturing, typically in high thermal flux environments that weaken the rocks surrounding the emplaced magma [Jaeger *et al.*, 2009; Hickey *et al.*, 2015; Acocella, 2021]. A lack of reservoir fracturing, and subsequent dyke emplacement, could also explain the low level of eruptive activity during the observed deformation period, despite the steady ground inflation (Figure 4.2). Thermal alterations to enable aseismic deformation requires the inclusion of time dependent, viscoelastic rock behaviours in any modelling work [Newman *et al.*, 2001; Gottsmann *et al.*, 2014; Head *et al.*, 2019]. These viscoelastic behaviours were not featured in this study, as only elastic rheologies were considered, with future analyses benefitting from

the inclusion of the temporal effects that can account for aseismic deformation.

4.4.2 Shallow Source Overpressure

The best fit shallow pressure source yielded an overpressure of 50 MPa, exceeding estimated values at which failure is believed to occur in magmatic reservoirs, the result of which is likely to be dyke emplacement; previous studies suggested a range of 0.5 – 9 MPa [Gudmundsson, 2006, 2012]. This failure range was estimated from shallow in-situ analyses, with laboratory-based results yielding maximum overpressures of around 31 MPa before failure occurs [Zhang, 2002; Smith *et al.*, 2009]. An important consideration is that the models in this study do not incorporate viscoelasticity. High geothermal gradients around magmatic reservoirs can cause the surrounding rocks to deform inelastically [Newman *et al.*, 2001; Head *et al.*, 2019; Heap *et al.*, 2021]. If a viscoelastic rheology for these rocks is assumed, source overpressure requirements can be reduced compared with those in purely elastic settings [Del Negro *et al.*, 2009; Gregg *et al.*, 2013; Hickey *et al.*, 2016; Cabaniss *et al.*, 2020], in some cases by as much as 40% [Hickey *et al.*, 2013]. A 40% reduction in overpressure at Sakurajima returns a value of 30 MPa, below the laboratory-based failure value of 31 MPa [Zhang, 2002].

4.4.3 Applicability of Gravity Modelling Approach

The gravity modelling in this study highlighted the possibility of using extensive Bouguer anomaly data at Aira caldera. Misfit analysis was conducted, using three different shallow source locations (deformation best fit, Minamidake, and the Sakurajima -10 mGal anomaly), and a range of density contrasts between the shallow and deep sources and the immediately adjacent crust. The modelled Bouguer anomaly distribution from the shallow -10 mGal anomaly source, using a density contrast of 500 kg/m³ between source and crust, produced the 'best' fit. However, none of the three locations assessed provide a good fit to the measured data, regardless of the density contrast used, with large areas of misfit over Kagoshima Bay, and the northern flank of Sakurajima. With the current tested parameter ranges, the methods used for gravity modelling in this study were unable to better determine a realistic shallow magmatic source location due to the high levels of misfit.

In the gravity modelling, subsurface properties, such as density and Young's Modulus, inferred from 3D seismic tomography data acquired in an expansive regional study [Alanis *et al.*, 2012; Hickey *et al.*, 2016], failed to provide high spatial resolutions for shallow depth locations. Additional steps should be taken to improve the accuracy and sensitivity of model parameters at shallow depths for future modelling studies using gravity-based methods at Sakurajima. The inclusion of small-scale local seismic tomography surveys [e.g., Miyamachi *et al.*, 2013; Tsutsui *et al.*, 2013] would add increased parameter resolution in the shallower regions beneath Aira caldera and Sakurajima volcano.

Another possible solution to improve model results is to consider the geology of the volcanic edifice and very upper crust, as opposed to having a total reliance on 3D seismic velocities. Sakurajima possesses a range of lithologies including lavas, pumices, and pyroclastic materials, as shown by borehole core samples from around the edifice, which highlight the variety of products from the volcano's eruptive past [Uto *et al.*, 1999; Miki *et al.*, 2000; Aizawa *et al.*, 2011]. Densities can be estimated by understanding what lithologies are present. The combination of lithology estimated densities for the edifice and seismic inferred equivalents at greater depths could produce a more accurate base for future gravity modelling studies at Sakurajima.

4.4.4 Other Limitations

There are numerous discrepancies between measured and modelled horizontal displacements, particularly on the north-eastern side of the Sakurajima edifice. A magmatic pathway, through a NE-SW striking structure, has been suggested previously to account for this, that could produce significant horizontal displacements capable of accounting for the displacement discrepancies observed [Hidayati *et al.*, 2007; Hickey *et al.*, 2016]. A double source model including this proposed pathway may output displacements that better represent the measured data from the magmatic system.

An assumption for this study was the fact the deep pressure source parameters, representing the optimal single source solution [Hickey *et al.*, 2016], were kept constant throughout. Primary magmatic reservoirs are known to dominate measured displacement patterns during deformation episodes, due to the significantly larger source having increased surface contact with the adjacent

crust [Okada, 1992; Dzurisin, 2007]. By using the single deep source solution to search for a secondary shallower source, any unresolved displacement errors in the original study are compounded. Altering the modelling approach to vary both shallow and deep source parameters, despite the increased computation time to reflect the greater number of potential magmatic system arrangements, would allow the existence and potential parameters of additional pressure sources to be verified independently of previous modelling results.

4.5 Conclusions

Numerical modelling of volcanic surface deformation, assuming a multiple pressure source system, has been conducted for the first time at Aira caldera. Efforts to improve on first order analytical studies [Iguchi *et al.*, 2008; Iguchi, 2013; Yamamoto *et al.*, 2013; Hotta *et al.*, 2016] that dominated the literature for the Aira caldera and Sakurajima volcano, have built on an initial single source numerical study [Hickey *et al.*, 2016], which used deformation data from 1996 – 2007 to locate and constrain a potential shallow pressure source beneath the Sakurajima volcanic edifice. The numerical modelling results presented here show:

- A double pressure source system produces a better fit to measured deformation data between 1996 – 2007 than a single source system.
- The best fit deformation solution for the secondary pressure source is prolate shaped (semi-major axis = 0.347 km, semi-minor axis = 1.040 km), and situated 2.8 km northwest of the Minamidake vent ($X = 130^{\circ} 38' 27.55''$, $Y = 31^{\circ} 35' 53.89''$, $Z = 7$ km), contrasting with previous analytical estimates of a shallow pressure source beneath the active Minamidake vent.
- The best fit gravity solution is located beneath the -10 mGal anomaly 1.7 km north of Minamidake ($X = 130^{\circ} 39' 36.60''$, $Y = 31^{\circ} 35' 39.49''$), with a 500 kg/m^3 density contrast between the two sources and the surrounding crust.
- Differences remain between the measured data and the modelled deformation predictions. It is feasible that more than two pressure sources

are present within the magmatic system, and possibly also a pressurized dyke between the two sources, supporting petrological and analytical modelling work which suggested that the Aira caldera magmatic system contains multiple pressure sources, or a trans-crustal magmatic system.

- Significant discrepancies exist between the modelled and measured gravity data, with all three coordinates used for the gravity modelling (Minamidake, deformation best fit, and the -10 mGal anomaly) poorly representing the observed data, regardless of the density contrast between the pressure sources and the adjacent crust.
- Future research should focus on the inclusion of additional pressure sources to account for discrepancies between modelled deformation results and measured data, and acquiring better resolution of shallow subsurface mechanical parameters (e.g., density and Young's Modulus) for improved deformation and gravity modelling.

Chapter 5:

Concluding Remarks

5.1 Thesis Summary

The primary goal of this thesis was to assess the complexity of the Aira caldera magmatic system in southern Kyushu, Japan. By independently modelling double magmatic source systems to assess the impact of varying pressure source parameters, a framework was developed to apply to the Aira caldera system. The models constructed used Finite Element (FE) modelling, integrating subsurface geological and geophysical attributes, to produce more accurate interpretations of surface deformation.

The investigation was initially carried out in 2D, evaluating how changing shallow source conditions in a generic model affected resulting surface displacements (Chapter 3). The results were then applied to Aira caldera, using a full 3D geometry to assess the potential for multiple pressure sources within the magmatic system (Chapter 4). Additional gravity modelling at Aira caldera incorporated measured and predicted subsurface density contrasts to further scrutinize the best fit shallow pressure source location against those estimated from previous work.

The 2D FE modelling, which assumed basic subsurface heterogeneity, highlighted the sensitivity of using predicted surface displacements to estimate depth and shape of a shallow source. From the differences in uplift produced by single and double source magmatic arrangements, deeper and larger reservoirs were found to dominate surface displacements in double source models, often preventing observation of contributions from a shallow source. From the evaluation of three different source shapes (oblate, prolate, and spherical), only shallow sources at the shallowest depths, with the largest volumes, and the highest overpressures, were detectable; oblate shallow sources produced the greatest uplift difference values.

The effect of source shape on spatial deformation fields is important, as the magnitudes and patterns of deformation reflect the different upward-facing surface areas in contact with the crust above a pressure source [Okada, 1992; Dzurisin, 2007; Hickey *et al.*, 2013]. Along with the effects of changing source shape, any variation in overpressure, depth, and volume of the shallow pressure sources, can change the displacement profiles, with modelling able to determine the scale of shallow magmatic structures, rate of magma accumulation, and

potential for eruptive activity.

For the first time, geodetic modelling of the Aira caldera and Sakurajima volcano magmatic system was conducted using numerical methods, assuming a multiple pressure source arrangement. Employing the optimal single source setup from the previous numerical study as a baseline [Hickey *et al.*, 2016], the new model improved the fit to the deformation data with the addition of a shallow pressure source 2.8 km northwest of the Minamidake vent. This result contrasts with previous location estimates of a shallow pressure source from analytical models, which suggested locations directly beneath the main eruptive vents [Yokoyama *et al.*, 1986; Eto, 1989; Iguchi, 2013; Hotta *et al.*, 2016]. This difference in location is potentially due to this study incorporating topography and subsurface heterogeneities, which have not previously been utilized in a double pressure source model. Discrepancies remain however between modelled and measured displacements, notably in the horizontal displacements on the north-eastern flank of Sakurajima, suggesting that the best fit deformation solution was not entirely accurate. Despite the double source arrangement providing a better data fit than the single source model, the remaining discrepancies imply the optimal modelled arrangement can be further refined, for example by the inclusion of additional pressure sources and connective magmatic pathways, or incorporating viscoelastic material behaviours.

The optimal gravity solution for a shallow source was located 1.7 km north of Minamidake, with a density contrast between the two pressure sources and the surrounding crust of 500 kg/m^3 . However, every set of shallow source coordinates and density contrasts used produced poor fits to the measured gravity data, with major differences in resultant modelled surface gravity fields. The poor data fits may be explained by low resolutions within the seismic tomography data used to infer the shallow subsurface density distribution. Future gravity modelling at Sakurajima should therefore incorporate local, high-resolution surveys, and density estimations from known lithological components of the volcanic edifice.

Despite the advancements made over the previous numerical model for Sakurajima volcano, simply using subsurface heterogeneity to increase model accuracy is not sufficient to fully assess the complexity of the Aira caldera magmatic system, or other magmatic systems world-wide. The inclusion of

viscoelastic crustal components, combined with more precise shallow subsurface density estimates, presents the means to improve future geodetic modelling across a range of magmatic systems.

To return to the title question of this thesis, Aira caldera possesses a highly complex magmatic system, likely containing at least a main magmatic reservoir beneath Aira caldera, and a secondary shallower reservoir beneath the active vent of Sakurajima volcano. The modelling work presented at Aira caldera represents a trade-off between computation time, model element size, and the precision of surface and subsurface topographies and mechanical properties. Combined, these factors mean only a certain level of complexity can be justified within the magmatic system. The addition of a secondary shallow source to the previously modelled deep primary reservoir [Hickey *et al.*, 2016] is a complexity that can be fully justified due to data misfits from the initial study, with seismic and petrological results also indicating shallow magma storage [Zawalna-Geer *et al.*, 2019; Brown *et al.*, 2020]. However, the improvement of data fit between the single and double source models is marginal, and large misfits are still present. Enhancements and additions, building on the limitations in precision of subsurface mechanical properties, and constant improvement of computational prowess, represent methods of advancement, however the scale of the data fit improvement is unknown. The remaining misfits are significant enough to warrant the continued addition of complexities, and the sustained emphasis on geodetic modelling at Aira caldera.

5.2 Implications and Limitations

5.2.1 Crustal Rheology

The literature on deformation modelling at Sakurajima is dominated by analytical approaches, which use single or multiple pressure sources to assess deformation episodes [Iguchi *et al.*, 2008; Iguchi, 2013; Hotta *et al.*, 2016]. This thesis favours a higher complexity numerical approach to overcome the limitations of analytical methods, namely the failure to incorporate crustal heterogeneities caused by variations in crustal mechanical properties in the crust.

Modelling throughout this thesis assumed an elastic rheology, where an applied stress causes an immediate reaction from the material, and once this stress is

removed, the material regains its original shape [Ranalli, 1995; Acocella, 2021]. The relationship between the direct proportion of stress and strain is time independent, and whilst providing a simple representation of crustal characteristics, it likely fails to accurately represent true complexities of rock behaviour in all circumstances. The lithosphere typically displays viscoelastic deformation, where strain accumulates with time, and deformation of the material is not fully recoverable [Fung, 1965; Ranalli, 1995; Christensen, 2003]. There are further complications in volcanic regions, such as elevated geothermal gradients, especially in long lived magmatic systems or at shallow depths [Annen, 2011; Karakas *et al.*, 2017], where the proximity of high temperature magmatic systems to surrounding rocks can alter the way rocks deform [Newman *et al.*, 2001; Heap *et al.*, 2021]. Temperature exercises a strong control on viscosity, amongst other properties [Ranalli, 1995; Smith *et al.*, 2009; Head *et al.*, 2019], so full implementation of time-dependent deformation phenomena can represent magmatic systems more realistically. Viscoelastic material properties, however, can be the result of estimations, either from geophysical observations or experiments. Any lack of understanding of how these input values change may impact the overall modelling results.

The lack of viscoelastic materials in the modelling approach at Aira caldera may have impacted on the assessment of shallow source location and parameters, although this could only be confirmed by repeating the same modelling assuming viscoelasticity throughout. The high overpressure (50 MPa) of our estimated shallow source could be affected by considering a viscoelastic medium, reducing the pressure requirement down to expected levels prior to rock failure [Zhang, 2002; Hickey *et al.*, 2013]. Another major simplification is representing magma reservoirs as hollow, static, overpressurized cavities [e.g., Currenti *et al.*, 2014; Hickey *et al.*, 2016, 2020; Head *et al.*, 2019; Gottsmann *et al.*, 2020]. It would be better to replace these cavities with rheological materials and a set of boundary conditions capable of mimicking magma flux, which is more realistic to the realistic dynamic nature of magma supply and accumulation [Le Mével *et al.*, 2016; Liao *et al.*, 2021].

5.2.2 Combined Deformation and Gravity Modelling

Chapter 4 of this thesis used Bouguer gravity anomaly distributions to scrutinize

potential shallow pressure source coordinates and parameters beneath Sakurajima. Modelled gravity changes can be compared to measured data, alongside surface displacement measurements, aiding in constraining source parameters (location, volume, depth, etc) as the subsurface density distribution is altered by magma flux [*Battaglia et al.*, 2009]. However, the deformation and gravity modelling in this thesis were conducted separately, with no link between resultant pressure source volume change, and its effects on the modelled gravity distribution [e.g., *Currenti*, 2018; *Gottsmann et al.*, 2020].

A risk in geodetic modelling is assuming that all deformation recorded during a period of activity is of magmatic origin. Deformation in volcanic regions can often be non-magmatic (e.g., hydrothermal, or volcanic edifice instabilities) [e.g., *Bonaccorso et al.*, 2013; *Kereszturi et al.*, 2021], with microgravity modelling able to discern between resulting deformation profiles of varying causes [*Battaglia et al.*, 2009; *Fernández et al.*, 2017]. Modelling of deformation only, such as in this thesis, may therefore provide inaccurate shallow source parameters. Our subsequent gravity modelling, utilizing the best fit shallow source from the deformation, yielded a different optimal shallow source location. However, the high overall level of misfit across all tested source coordinates, highlights the challenges with the resolution of the subsurface density distribution used. A coupled deformation and gravity modelling approach to accommodate changes in magma flux and potential viscoelastic rheologies, with equivalent time-varying surface displacement and Bouguer anomaly data, might present an optimal method to estimate shallow magmatic storage locations and sizes during unrest episodes.

5.2.3 Multiple Pressure Source Modelling

The multiple pressure source numerical modelling conducted in this thesis is the first such study of its kind conducted at Sakurajima. By using a set number of reservoirs, the deformation modelling conducted assumed that all modelled surface displacements were from a finite number of focussed areas within the subsurface. The location of the best fit shallow pressure source beneath Sakurajima is laterally offset from the active vent and any observed seismic activity, which could suggest either: 1) recorded deformation has both magmatic and non-magmatic origins, or 2) more than two pressure sources are present.

Modern interpretations of magmatic systems imply significantly greater complexities, such magma-crystal mush transcrustal magmatic systems (TCMS) [Cashman *et al.*, 2014; Hammond *et al.*, 2019]. Mush-dominated models have grown in popularity due to geochemical evidence of inconsistent mineral assemblages and process inferences that are incompatible with isolated magmatic sources [Zawalna-Geer *et al.*, 2019; Brown *et al.*, 2020]. The potential for a crystalline mush to alter stress transfer rates from a magma reservoir to the surrounding crust [e.g., Cashman *et al.*, 2017; Sparks *et al.*, 2017; Singer *et al.*, 2018], could produce different surface displacements compared to a simple melt-dominated reservoir.

A TCMS style arrangement could account for some of the issues from the Sakurajima modelling, notably the potential for more than two pressure sources. Despite lacking a clearly defined magmatic chamber and the surrounding crust, the geometries of TCMS pressure sources could be assumed to reflect the volume of a crystalline magma-mush reservoir, not representing a large volume of liquid magma. Basic geophysical modelling of vertically extensive pseudo-TCMS style arrangements has been conducted [e.g., Gottsmann, *et al.*, 2020], but accounting for the complexities in melt volumes, overpressure ranges, and overall irregularities has hampered modelling efforts to date.

The ability for Finite Element models, however, to account for complex shapes, boundaries, and coupled solid and fluid mechanics, means advancements in TCMS understanding can be further explored with geophysical modelling. Such improvements, when applied to a volcanic system such as Sakurajima, which is already hypothesised to possess a TCMS [Zawalna-Geer *et al.*, 2019; Brown *et al.*, 2020], combined with poroelastic deformation modelling [Liao *et al.*, 2021], may alter the way future deformation is interpreted, positively impacting future eruption forecasts and hazard assessments.

5.3 Future Applications

The required level of additional information needed for complex, volcano-specific 3D numerical modelling, such as subsurface densities, elastic parameters, rheologies, surface topographies and bathymetries, still limits the potential for numerical approaches to be applied worldwide. An analytical approach, despite the potential for inaccuracies in source parameter estimates, is still often the only

viable method in scenarios such as in rapid response to a poorly understood volcanic system. The high cost of obtaining sufficient subsurface information for every potentially active volcano worldwide for full application of numerical techniques, makes this not viable. Volcanoes near large population centers, and where sufficient funding exists to conduct the required geophysical surveys, are prime targets for numerical modelling. Access to the required computational power to numerically model deformation is becoming less of a challenge, as computer codes become more efficient, and there is a reduction in the cost of high-performance computing.

Despite improved interpretations of locations and parameters of causative shallow pressure sources within magmatic systems, additional advancements can be made to improve the future study of volcano deformation at Sakurajima. A more accurate model of deformation at Sakurajima could be accomplished by the inclusion of additional factors: 1) utilizing viscoelastic rheologies and multiple pressure sources, 2) concurrent deformation and gravity data to correlate temporal changes, 3) higher resolution seismic tomography surveys for higher precision inferred subsurface density distributions, 4) density estimates of edifice lithologies, and 5) coupling of solid-fluid mechanics and poroelastic reservoirs, to characterize potential mush-dominated magmatic systems. Combined, these considerations should create a more accurate representation of subsurface heterogeneities beneath Sakurajima, improving on location and scale estimates of shallow magmatic storage. The higher accuracy potential of numerical modelling techniques highlights its effectiveness for volcanic hazard monitoring. Uncertainties in producing exact representations of crustal characteristics currently restricts the full potential of geodetic modelling. However, the modelling framework is clearly in place for application of improvements and new findings to enable comprehensive deformation interpretations in the future.

References

- Acocella, V. (2021) *Volcano-Tectonic Processes*. Springer Nature.
- Aizawa, K., Kanda, W., Ogawa, Y., Iguchi, M., Yokoo, A., Yakiwara, H. and Sugano, T. (2011) 'Temporal changes in electrical resistivity at Sakurajima volcano from continuous magnetotelluric observations', *Journal of volcanology and Geothermal Research*. Elsevier, 199(1–2), pp. 165–175.
- Alanis, P., Miyamachi, H., Yakiwara, H., Goto, K., Kobayahsi, R., Tameguri, T. and Iguchi, M. (2012) 'Seismic Velocity Structure of the Crust Beneath the Aira Caldera in Southern Kyushu by Tomography of Travel Times of Local Earthquake Data', *Bulletin of the Volcanological Society of Japan*, 57(4), pp. 227–234. doi: 10.18940/kazan.57.4_227.
- Annen, C. (2011) 'Implications of incremental emplacement of magma bodies for magma differentiation, thermal aureole dimensions and plutonism–volcanism relationships', *Tectonophysics*. Elsevier, 500(1–4), pp. 3–10.
- Aramaki, S. (1984) 'Formation of the Aira Caldera , Southern Kyushu, ~22'000 Years Ago', *Journal of Geophysical Research*, 89(4), pp. 8485–8501.
- Araya, N., Nakamura, M., Yasuda, A., Okumura, S., Sato, T., Iguchi, M., Miki, D. and Geshi, N. (2019) 'Shallow magma pre-charge during repeated Plinian eruptions at Sakurajima volcano', *Scientific Reports*. Springer US, 9(1), pp. 1–10. doi: 10.1038/s41598-019-38494-x.
- Bagnardi, M., Poland, M. P., Carbone, D., Baker, S., Battaglia, M. and Amelung, F. (2014) 'Gravity changes and deformation at Kilauea Volcano, Hawaii, associated with summit eruptive activity, 2009–2012', *Journal of Geophysical Research: Solid Earth*. Wiley Online Library, 119(9), pp. 7288–7305.
- Battaglia, M., Gottsmann, J., Carbone, D. and Fernández, J. (2008) '4D volcano gravimetry', *Geophysics*, 73(6). doi: 10.1190/1.2977792.
- Battaglia, M. and Hill, D. P. (2009) 'Analytical modeling of gravity changes and crustal deformation at volcanoes: The Long Valley caldera, California, case study', *Tectonophysics*. Elsevier B.V., 471(1–2), pp. 45–57. doi: 10.1016/j.tecto.2008.09.040.
- Biggs, J., Ebmeier, S. K., Aspinall, W. P., Lu, Z., Pritchard, M. E., Sparks, R. S. J. and Mather, T. A. (2014) 'Global link between deformation and volcanic eruption quantified by satellite imagery', *Nature communications*. Nature Publishing Group, 5(1), pp. 1–7.
- Biggs, J. and Pritchard, M. E. (2017) 'Global volcano monitoring: What does it mean when volcanoes deform?', *Elements*, 13(1), pp. 17–22. doi: 10.2113/gselements.13.1.17.
- Bonaccorso, A., Currenti, G. and Del Negro, C. (2013) 'Interaction of volcano-tectonic fault with magma storage, intrusion and flank instability: A thirty years study at Mt. Etna volcano', *Journal of Volcanology and Geothermal Research*. Elsevier, 251, pp. 127–136.
- Bonaccorso, A. and Davis, P. M. (1999) 'Models of ground deformation from vertical volcanic conduits with application to eruptions of Mount St. Helens and Mount Etna', *Journal of Geophysical Research: Solid Earth*. Wiley Online Library, 104(B5), pp. 10531–10542.
- Brocher, T. M. (2005) 'Empirical relations between elastic wavespeeds and density in the Earth's crust', *Bulletin of the seismological Society of America*. Seismological Society of America, 95(6), pp. 2081–2092.
- Brown, J. R., Taylor, R. N. and Iguchi, M. (2020) 'Using high-resolution Pb isotopes to unravel the petrogenesis of Sakurajima volcano, Japan', *Bulletin of Volcanology*. Bulletin of Volcanology, 82(5). doi: 10.1007/s00445-020-1371-0.
- Bürgmann, R., Rosen, P. A. and Fielding, E. J. (2000) 'Synthetic aperture radar interferometry to measure Earth's surface topography and its deformation', *Annual review of earth and planetary sciences*. Annual Reviews 4139 El Camino Way, PO Box 10139, Palo Alto, CA 94303-0139, USA, 28(1), pp. 169–209.
- Cabaniss, H. E., Gregg, P. M., Nooner, S. L. and Chadwick, W. W. (2020) 'triggering of eruptions at Axial Seamount, Juan de fuca Ridge', *Scientific reports*. Nature Publishing Group, 10(1), pp. 1–11.

References

- Cai, Y. and Wang, C. Y. (2005) 'Fast finite-element calculation of gravity anomaly in complex geological regions', *Geophysical Journal International*, 162(3), pp. 696–708. doi: 10.1111/j.1365-246X.2005.02711.x.
- Cashman, K. V., Sparks, R. S. J. and Blundy, J. D. (2017) 'Vertically extensive and unstable magmatic systems: A unified view of igneous processes', *Science*, 355(6331). doi: 10.1126/science.aag3055.
- Cashman, K. V and Giordano, G. (2014) 'Calderas and magma reservoirs', *Journal of Volcanology and Geothermal Research*. Elsevier, 288, pp. 28–45.
- Cashman, K. V and Sparks, R. S. J. (2013) 'How volcanoes work: A 25 year perspective', *GSA bulletin*. GeoScienceWorld, 125(5–6), pp. 664–690.
- Christensen, R. M. (2003) 'Theory of Viscoelasticity (Dover, New York)'.
- Currenti, G. (2014) 'Numerical evidence enabling reconciliation of gravity and height changes in volcanic areas', *Geophysical Journal International*, 197(1), pp. 164–173. doi: 10.1093/gji/ggt507.
- Currenti, G. (2018) 'Viscoelastic modeling of deformation and gravity changes induced by pressurized magmatic sources', *Journal of Volcanology and Geothermal Research*. Elsevier B.V., 356, pp. 264–277. doi: 10.1016/j.jvolgeores.2018.03.020.
- Currenti, G., Del Negro, C. and Ganci, G. (2007) 'Modelling of ground deformation and gravity fields using finite element method: An application to Etna volcano', *Geophysical Journal International*, 169(2), pp. 775–786. doi: 10.1111/j.1365-246X.2007.03380.x.
- Currenti, G., Del Negro, C. and Ganci, G. (2008) 'Finite element modeling of ground deformation and gravity field at Mt. Etna', *Annals of Geophysics*, 51(1), pp. 105–119. doi: 10.4401/ag-3037.
- Currenti, G. and Williams, C. A. (2014) 'Numerical modeling of deformation and stress fields around a magma chamber: Constraints on failure conditions and rheology', *Physics of the Earth and Planetary Interiors*. Elsevier B.V., 226, pp. 14–27. doi: 10.1016/j.pepi.2013.11.003.
- Desai, B., Maskrey, A., Peduzzi, P., De Bono, A. and Herold, C. (2015) 'Making development sustainable: the future of disaster risk management, global assessment report on disaster risk reduction'. United Nations Office for Disaster Risk Reduction (UNISDR).
- Dieterich, J. and Decker, R. (1975) 'Finite Element Modeling of Surface Deformation Associated With Volcanism', *Journal of Geophysical Research*, 80(29), pp. 4094–4102.
- Dvorak, J. J. and Dzurisin, D. (1997) 'Volcano geodesy: The search for magma reservoirs and the formation of eruptive vents', *Reviews of Geophysics*. Blackwell Publishing Ltd, 35(3), pp. 343–384. doi: 10.1029/97RG00070.
- Dzurisin, D. (1992) 'Electronic tiltmeters for volcano monitoring: lessons from Mount St. Helens', *US Geol. Surv. Bull.*, 1966, pp. 69–83.
- Dzurisin, D. (2003) 'A comprehensive approach to monitoring volcano deformation as a window on the eruption cycle', *Reviews of Geophysics*, 41(1), pp. 1–29. doi: 10.1029/2001RG000107.
- Dzurisin, D. (2007) *Volcano deformation: Geodetic monitoring techniques*. Praxis Publishing, Chichester.
- Dzurisin, D., Donnelly-Nolan, J. M., Evans, J. R. and Walter, S. R. (1991) 'Crustal subsidence, seismicity, and structure near Medicine Lake volcano, California', *Journal of Geophysical Research: Solid Earth*. Wiley Online Library, 96(B10), pp. 16319–16333.
- Dzurisin, D., Poland, M. P. and Bürgmann, R. (2002) 'Steady subsidence of Medicine Lake volcano, northern California, revealed by repeated leveling surveys', *Journal of Geophysical Research: Solid Earth*. Wiley Online Library, 107(B12), p. ECV-8.
- Ebmeier, S. K., Andrews, B. J., Araya, M. C., Arnold, D. W. D., Biggs, J., Cooper, C., Cottrell, E., Furtney, M., Hickey, J., Jay, J., Lloyd, R., Parker, A. L., Pritchard, M. E., Robertson, E., Venzke, E. and Williamson, J. L. (2018) 'Synthesis of global satellite observations of magmatic and volcanic deformation: implications for volcano monitoring & the lateral extent of magmatic domains', *Journal of Applied Volcanology*. Journal of Applied Volcanology, 7(1), pp. 1–26. doi: 10.1186/s13617-018-0071-3.
- Eto, T. (1989) 'Ground deformation at Sakurajima and around Aira caldera associated with the volcanic activity.', *Ann. Disaster Prev. Res. Inst., Kyoto Univ.* 京都大学防災研究所, 32, pp. 29–

References

- 39.
- Fernández, J., Pepe, A., Poland, M. P. and Sigmundsson, F. (2017) 'Volcano Geodesy: Recent developments and future challenges', *Journal of Volcanology and Geothermal Research*. Elsevier, 344, pp. 1–12.
- Fialko, Y., Khazan, Y. and Simons, M. (2001) 'Deformation due to a pressurized horizontal circular crack in an elastic half-space, with applications to volcano geodesy', *Geophysical Journal International*. Blackwell Publishing Ltd Oxford, UK, 146(1), pp. 181–190.
- Fung, Y. (1965) 'Foundations of solid mechanics(Book on deformation and motion of elastic and plastic solids including variational calculus and tensor analysis)', *ENGLEWOOD CLIFFS, N. J., PRENTICE-HALL, INC., 1965. 525 P.*
- Geudtner, D., Torres, R., Snoeij, P., Davidson, M. and Rommen, B. (2014) 'Sentinel-1 system capabilities and applications', in *2014 IEEE Geoscience and Remote Sensing Symposium*. IEEE, pp. 1457–1460.
- Geyer, A. and Gottsmann, J. (2010) 'The influence of mechanical stiffness on caldera deformation and implications for the 1971–1984 Rabaul uplift (Papua New Guinea)', *Tectonophysics*. Elsevier, 483(3–4), pp. 399–412.
- Gottsmann, J., Biggs, J., Lloyd, R., Biranhu, Y. and Lewi, E. (2020) 'Ductility and Compressibility Accommodate High Magma Flux Beneath a Silicic Continental Rift Caldera: Insights From Corbetti Caldera (Ethiopia)', *Geochemistry, Geophysics, Geosystems*, 21(4). doi: 10.1029/2020GC008952.
- Gottsmann, J., Carniel, R., Coppo, N., Wooller, L., Hautmann, S. and Rymer, H. (2007) 'Oscillations in hydrothermal systems as a source of periodic unrest at caldera volcanoes: Multiparameter insights from Nisyros, Greece', *Geophysical Research Letters*. Wiley Online Library, 34(7).
- Gottsmann, J., Flynn, M. and Hickey, J. (2020) 'The Transcrustal Magma Reservoir Beneath Soufrière Hills Volcano, Montserrat: Insights From 3-D Geodetic Inversions', *Geophysical Research Letters*, 47(20). doi: 10.1029/2020GL089239.
- Gottsmann, J., Folch, A. and Rymer, H. (2006) 'Unrest at Campi Flegrei: A contribution to the magmatic versus hydrothermal debate from inverse and finite element modeling', *Journal of Geophysical Research*, 111(B7), pp. 1–11. doi: 10.1029/2005jb003745.
- Gottsmann, J. and Odbert, H. (2014) 'The effects of thermomechanical heterogeneities in island arc crust on time-dependent preeruptive stresses and the failure of an andesitic reservoir', *Journal of Geophysical Research: Solid Earth*. Wiley Online Library, 119(6), pp. 4626–4639.
- Gottsmann, J. and Rymer, H. (2002) 'Deflation during caldera unrest: constraints on subsurface processes and hazard prediction from gravity–height data', *Bulletin of Volcanology*. Springer, 64(5), pp. 338–348.
- Gregg, P. M., De Silva, S. L. and Grosfils, E. B. (2013) 'Thermomechanics of shallow magma chamber pressurization: Implications for the assessment of ground deformation data at active volcanoes', *Earth and Planetary Science Letters*. Elsevier, 384, pp. 100–108.
- Gregg, P. M., De Silva, S. L., Grosfils, E. B. and Parmigiani, J. P. (2012) 'Catastrophic caldera-forming eruptions: Thermomechanics and implications for eruption triggering and maximum caldera dimensions on Earth', *Journal of Volcanology and Geothermal Research*. Elsevier, 241, pp. 1–12.
- Grosfils, E. B. (2007) 'Magma reservoir failure on the terrestrial planets: Assessing the importance of gravitational loading in simple elastic models', *Journal of Volcanology and Geothermal Research*. Elsevier, 166(2), pp. 47–75.
- Gudmundsson, A. (2005) 'The effects of layering and local stresses in composite volcanoes on dyke emplacement and volcanic hazards', *Comptes Rendus Geoscience*. Elsevier, 337(13), pp. 1216–1222.
- Gudmundsson, A. (2006) 'How local stresses control magma-chamber ruptures, dyke injections, and eruptions in composite volcanoes', *Earth-Science Reviews*, 79(1–2), pp. 1–31. doi: 10.1016/j.earscirev.2006.06.006.
- Gudmundsson, A. (2009) 'Toughness and failure of volcanic edifices', *Tectonophysics*, 471, pp. 27–35. doi: 10.1016/j.tecto.2009.03.001.

References

- Gudmundsson, A. (2011) *Rock fractures in geological processes*. Cambridge University Press.
- Gudmundsson, A. (2012) 'Magma chambers: Formation, local stresses, excess pressures, and compartments', *Journal of Volcanology and Geothermal Research*. Elsevier B.V., 237–238, pp. 19–41. doi: 10.1016/j.jvolgeores.2012.05.015.
- Gudmundsson, M. T., Jónsdóttir, K., Hooper, A., Holohan, E. P., Halldórsson, S. A., Ófeigsson, B. G., Cesca, S., Vogfjörð, K. S., Sigmundsson, F. and Högnadóttir, T. (2016) 'Gradual caldera collapse at Bárðarbunga volcano, Iceland, regulated by lateral magma outflow', *Science*. American Association for the Advancement of Science, 353(6296).
- Hamling, I. J., Hreinsdóttir, S. and Fournier, N. (2015) 'The ups and downs of the TVZ: Geodetic observations of deformation around the Taupo Volcanic Zone, New Zealand', *Journal of Geophysical Research: Solid Earth*. Wiley Online Library, 120(6), pp. 4667–4679.
- Hammond, J. O. S., Wu, J., Ri, K., Wei, W. and Yu, J. (2019) 'Distribution of Partial Melt Beneath Changbaishan / Paektu Volcano, China / Democratic People's Republic of Korea', pp. 1–17. doi: 10.1029/2019GC008461.
- Hautmann, S., Gottsmann, J., Sparks, R. S. J., Mattioli, G. S., Sacks, I. S. and Strutt, M. H. (2010) 'Effect of mechanical heterogeneity in arc crust on volcano deformation with application to Soufrière Hills Volcano, Montserrat, West Indies', *Journal of Geophysical Research: Solid Earth*. Wiley Online Library, 115(B9).
- Head, M., Hickey, J., Gottsmann, J. and Fournier, N. (2019) 'The Influence of Viscoelastic Crustal Rheologies on Volcanic Ground Deformation: Insights From Models of Pressure and Volume Change', *Journal of Geophysical Research: Solid Earth*, 124(8), pp. 8127–8146. doi: 10.1029/2019JB017832.
- Heap, M. J. and Violay, M. E. S. (2021) 'The mechanical behaviour and failure modes of volcanic rocks: a review', *Bulletin of Volcanology*. Springer, 83(5), pp. 1–47.
- Hickey, J. and Gottsmann, J. (2014) 'Benchmarking and developing numerical Finite Element models of volcanic deformation', *Journal of Volcanology and Geothermal Research*. Elsevier B.V., 280, pp. 126–130. doi: 10.1016/j.jvolgeores.2014.05.011.
- Hickey, J., Gottsmann, J. and Mothes, P. (2015) 'Estimating volcanic deformation source parameters with a finite element inversion: The 2001-2002 unrest at Cotopaxi volcano, Ecuador', *Journal of Geophysical Research: Solid Earth*, 120(3), pp. 1473–1486. doi: 10.1002/2014JB011731.
- Hickey, J., Gottsmann, J., Mothes, P., Odbert, H., Prutkin, I. and Vajda, P. (2017) 'The Ups and Downs of Volcanic Unrest: Insights from Integrated Geodesy and Numerical Modelling', in Gottsmann, J., Neuberg, J., and Scheu, B. (eds) *Volcanic Unrest: From Science to Society*. Cham: Springer International Publishing, pp. 203–219. doi: 10.1007/11157_2017_13.
- Hickey, J., Gottsmann, J., Nakamichi, H. and Iguchi, M. (2016) 'Thermomechanical controls on magma supply and volcanic deformation: Application to Aira caldera, Japan', *Scientific Reports*. Nature Publishing Group, 6(August), pp. 1–10. doi: 10.1038/srep32691.
- Hickey, J., Gottsmann, J. and Potro, R. (2013) 'The large-scale surface uplift in the Altiplano-Puna region of Bolivia: A parametric study of source characteristics and crustal rheology using finite element analysis', *Geochemistry, Geophysics, Geosystems*, 14(3), pp. 540–555. doi: 10.1002/ggge.20057.
- Hickey, J., Lloyd, R., Biggs, J., Arnold, D., Mothes, P. and Muller, C. (2020) 'Rapid localized flank inflation and implications for potential slope instability at Tungurahua volcano, Ecuador', *Earth and Planetary Science Letters*. Elsevier B.V., 534, p. 116104. doi: 10.1016/j.epsl.2020.116104.
- Hidayati, S., Ishihara, K. and Iguchi, M. (2007) 'Volcano-tectonic Earthquakes during the Stage of Magma Accumulation at the Aira Caldera, Southern Kyushu, Japan', *Bulletin of the Volcanological Society of Japan*, 52(6), pp. 289–309. doi: 10.18940/kazan.52.6_289.
- Hotta, K., Iguchi, M., Ohkura, T. and Yamamoto, K. (2016) 'Multiple-pressure-source model for ground inflation during the period of high explosivity at Sakurajima volcano, Japan - Combination analysis of continuous GNSS, tilt and strain data -', *Journal of Volcanology and Geothermal Research*. Elsevier B.V., 310, pp. 12–25. doi: 10.1016/j.jvolgeores.2015.11.017.
- Hotta, K., Iguchi, M. and Tameguri, T. (2016) 'Rapid dike intrusion into Sakurajima volcano on August 15, 2015, as detected by multi-parameter ground deformation observations', *Earth*,

References

- Planets and Space*. Springer Berlin Heidelberg, 68(1). doi: 10.1186/s40623-016-0450-0.
- IAVCEI Subcommittee on Decade Volcanoes (1994) 'Research at Decade Volcanos aimed at disaster prevention', *Eos, Transactions American Geophysical Union*. Wiley Online Library, 75(30), pp. 340–350.
- Iguchi, M. (2013) 'Magma Movement from the Deep to Shallow Sakurajima Volcano as Revealed by Geophysical Observations(Sakurajima Special Issue)', *Bulletin of the Volcanological Society of Japan*, 58(1), pp. 1–18. doi: 10.18940/kazan.58.1_1.
- Iguchi, M., Takayama, T., Yamazaki, T., Tada, M., Suzuki, A., Ueki, S., Ohta, Y. and Nakao, S. (2008) 'Movement of magma at Sakurajima Volcano revealed by GPS observation', *Annuals of Disaster Prevention Research Institute, Kyoto University*, 51, pp. 241–246.
- Iguchi, M., Tameguri, T., Ohta, Y., Ueki, S. and Nakao, S. (2013) 'Characteristics of Volcanic Activity at Sakurajima Volcano 's Showa Crater During the Period 2006 to 2011', *Bulletin of the Volcanological Society of Japan*, 58(1), pp. 115–135.
- Ishihara, K. and Eto, T. (1978) 'Surface deformation associated with the eruptive activity at the summit crater of Sakurajima volcano.', *Ann. Disaster Prev. Res. Inst., Kyoto Univ.* 京都大学防災研究所, 21, pp. 153–162.
- Ishihara, K., Takayama, K., Tanaka, Y. and Hirabayashi, J.-L. (1981) 'Lava flows at Sakurajima volcano (I), volume of the historical lava flows', *Annuals Disaster Prevention Research Institute, Kyoto University, Kyoto*, 24(1), pp. 1–10.
- Ishikawa, N. (1997) 'Differential rotations of north Kyushu Island related to middle Miocene clockwise rotation of SW Japan', *Journal of Geophysical Research: Solid Earth*. Wiley Online Library, 102(B8), pp. 17729–17745.
- Jaeger, J. C., Cook, N. G. W. and Zimmerman, R. (2009) *Fundamentals of rock mechanics*. John Wiley & Sons.
- Jing, L. and Hudson, J. A. (2002) 'Numerical methods in rock mechanics', *International Journal of Rock Mechanics and Mining Sciences*, 39(4), pp. 409–427. doi: 10.1016/S1365-1609(02)00065-5.
- Johnson, J. H., Poland, M. P., Anderson, K. R. and Biggs, J. (2019) 'A cautionary tale of topography and tilt from Kīlauea Caldera', *Geophysical Research Letters*. Wiley Online Library, 46(8), pp. 4221–4229.
- Kamata, H. and Kodama, K. (1999) 'Volcanic History and Tectonics of the Southwestern Japan Arc', in *The Island Arc*, pp. 393–403.
- Kaneko, T., Maeno, F. and Nakada, S. (2016) '2014 Mount Ontake eruption: Characteristics of the phreatic eruption as inferred from aerial observations the Phreatic Eruption of Mt. Ontake Volcano in 2014 5. Volcanology', *Earth, Planets and Space*. Springer Berlin Heidelberg, 68(1), pp. 1–11. doi: 10.1186/s40623-016-0452-y.
- Karakas, O., Degruyter, W., Bachmann, O. and Dufek, J. (2017) 'Lifetime and size of shallow magma bodies controlled by crustal-scale magmatism', *Nature Geoscience*. Nature Publishing Group, 10(6), pp. 446–450.
- Kereszturi, G., Schaefer, L., Mead, S., Miller, C., Procter, J. and Kennedy, B. (2021) 'Synthesis of hydrothermal alteration, rock mechanics and geophysical mapping to constrain failure and debris avalanche hazards at Mt. Ruapehu (New Zealand)', *New Zealand Journal of Geology and Geophysics*. Taylor & Francis, 0(0), pp. 1–22. doi: 10.1080/00288306.2021.1885048.
- Kobayashi, T. (2013) 'Geological Map of Sakurajima Volcano', *Geological Survey of Japan*.
- Kobayashi, T. and Tameike, T. (2002) 'History of eruptions and volcanic damage from Sakurajima volcano, southern Kyushu, Japan', *The Quaternary Research (Daiyonki-Kenkyu)*. Japan Association for Quaternary Research, 41(4), pp. 269–278.
- Kohno, Y., Matsushima, T. and Shimizu, H. (2008) 'Pressure sources beneath Unzen Volcano inferred from leveling and GPS data', *Journal of Volcanology and Geothermal Research*. Elsevier, 175(1–2), pp. 100–109.
- Komazawa, M., Hiroshima, T., Murata, Y., Morijiri, R. and Makino, M. (2000) 'Gravity Maps and CD-ROM of Japan by Geological Survey of Japan', *Geoinformatics*. Japan Society of Geoinformatics, 11(2), pp. 86–87.

References

- Komazawa, M., Nakamura, K., Yamamoto, K., Iguchi, M., Akamatsu, J., Ichikawa, N., Takayama, T. and Yamazaki, T. (2008) 'Gravity anomalies at Sakurajima volcano, southwest Japan', *Ann. Disast. Prev. Res. Inst., Kyoto Univ. B*, 51, pp. 261–266.
- LaFemina, P. C. (2015) 'Plate tectonics and volcanism', in *The encyclopedia of volcanoes*. Elsevier, pp. 65–92.
- Leick, A. (1990) 'GPS Satellite Surveying.', *Wiley Interscience*, 605, pp. 10012–10158.
- Liao, Y., Soule, S. A., Jones, M. and Le Mével, H. (2021) 'The mechanical response of a magma chamber with poroviscoelastic crystal mush', *Journal of Geophysical Research: Solid Earth*. Wiley Online Library, 126(4), p. e2020JB019395.
- Maeno, F. and Taniguchi, H. (2007) 'Spatiotemporal evolution of a marine caldera-forming eruption, generating a low-aspect ratio pyroclastic flow, 7.3 ka, Kikai caldera, Japan: Implication from near-vent eruptive deposits', 167, pp. 212–238. doi: 10.1016/j.jvolgeores.2007.05.003.
- Maruyama, S., Isozaki, Y., Kimura, G. and Terabayashi, M. (1997) 'Paleogeographic maps of the Japanese Islands: Plate tectonic synthesis from 750 Ma to the present', *Island Arc*, 6(1), pp. 121–142. doi: 10.1111/j.1440-1738.1997.tb00043.x.
- Massonnet, D. and Feigl, K. L. (1998) 'Radar interferometry and its application to changes in the Earth's surface', *Reviews of geophysics*. Wiley Online Library, 36(4), pp. 441–500.
- Massonnet, D., Rossi, M., Carmona, C., Adragna, F., Peltzer, G., Feigl, K. and Rabaute, T. (1993) 'The displacement field of the Landers earthquake mapped by radar interferometry', *nature*. Nature Publishing Group, 364(6433), pp. 138–142.
- Masterlark, T. (2007) 'Magma intrusion and deformation predictions: Sensitivities to the Mogi assumptions', *Journal of Geophysical Research: Solid Earth*, 112(6), pp. 1–17. doi: 10.1029/2006JB004860.
- McTigue, D. F. (1987) 'Elastic stress and deformation near a finite spherical magma body: Resolution of the point source paradox', *Journal of Geophysical Research*, 92(B12), p. 12931. doi: 10.1029/jb092ib12p12931.
- McTigue, D. F. and Segall, P. (1988) 'Displacements and tilts from dip-slip faults and magma chambers beneath irregular surface topography', *Geophysical Research Letters*. Wiley Online Library, 15(6), pp. 601–604.
- Le Mével, H., Gregg, P. M. and Feigl, K. L. (2016) 'Magma injection into a long-lived reservoir to explain geodetically measured uplift: Application to the 2007–2014 unrest episode at Laguna del Maule volcanic field, Chile', *Journal of Geophysical Research: Solid Earth*. Wiley Online Library, 121(8), pp. 6092–6108.
- Miki, D., Uto, K., Uchiumi, S. and Ishihara, K. (2000) 'K-Ar dating and paleomagnetic measurements on drilled cores from the Sakurajima volcano: Part 2', *Kyoto Daigaku Bōsai Kenkyūjo nenpō*, (43), pp. 1–6.
- Miyamachi, H. *et al.* (2013) 'Shallow Velocity Structure Beneath the Aira Caldera and Sakurajima Volcano as Inferred from Refraction Analysis of the Seismic Experiment in 2008', *Bulletin of the Volcanological Society of Japan*, 58(1), pp. 227–237.
- Miyamachi, H., Higashiura, K., Hirano, S. and Yamamoto, A. (2000) 'High density gravity measurements in Sakurajima volcano, southern Kyushu, Japan', *Kagoshima University Faculty of Science Bulletin*, 33, pp. 101–116.
- Mogi, K. (1958) 'Relations between the eruptions of various volcanoes and the deformations of the ground surfaces around them.', *Earthquake Research Institute*, pp. 99–134. doi: 10.1016/j.epsl.2004.04.016.
- Mori, N. *et al.* (2014) 'Nationwide post event survey and analysis of the 2011 Tohoku earthquake tsunami', *Coastal Engineering Journal*, 54(1). doi: 10.1142/S0578563412500015.
- Murata, Y., Nawa, K., Komazawa, M., Morijiri, R., Hiroshima, T., Makino, M., Yamazaki, T., Nishimura, K., Okuma, S. and Shichi, R. (2007) 'Bouguer Gravity Anomalies in Kagoshima District, Kyushu, Japan', *Bull. Geol. Surv. Japan*, 58, pp. 351–370.
- Nakagawa, M. (2011) 'Change of mode of eruptive activity and the magma plumbing system of Sakurajima Volcano since 20th century', in *Japan Geoscience Union Meeting 2001*. Makuhari.

References

- Nasu, N., Uyeda, S., Kobayashi, K., Kushiro, I. and Kagami, H. (1986) 'Formation of active ocean margins'. Springer, 20.
- Del Negro, C., Currenti, G. and Scandura, D. (2009) 'Temperature-dependent viscoelastic modeling of ground deformation: Application to Etna volcano during the 1993-1997 inflation period', *Physics of the Earth and Planetary Interiors*, 172(3–4), pp. 299–309. doi: 10.1016/j.pepi.2008.10.019.
- Newman, A. V, Dixon, T. H., Ofoegbu, G. I. and Dixon, J. E. (2001) 'Geodetic and seismic constraints on recent activity at Long Valley Caldera, California: evidence for viscoelastic rheology', *Journal of Volcanology and Geothermal Research*. Elsevier, 105(3), pp. 183–206.
- Odbert, H., Taisne, B. and Gottsmann, J. (2015) 'Deposit loading and its effect on co-eruptive volcano deformation', *Earth and Planetary Science Letters*. Elsevier, 413, pp. 186–196.
- Okada, Y. (1992) 'Internal deformation due to shear and tensile faults in a half-space', *Bulletin of the seismological society of America*. The Seismological Society of America, 82(2), pp. 1018–1040.
- Okuno, M. (2002) 'Chronology of tephra layers in southern Kyushu, SW Japan, for the Last 30,000 Years', *The Quaternary Research*, 41, pp. 223–236.
- Omori, F. (1916) 'The Sakura-jima eruptions and earthquakes. Part II.', *Bull. Imperial Earthq. Investigation Committee*, 8, pp. 5–152. Available at: <http://ci.nii.ac.jp/naid/10003670193/en/> (Accessed: 29 October 2019).
- Oramas-Dorta, D., Tirabassi, G., Franco, G. E. and Magill, C. (2019) 'Design of parametric risk transfer solutions for volcanic eruptions: an application to Japanese volcanoes', *Natural Hazards and Earth System Sciences Discussions*. Copernicus GmbH, pp. 1–32.
- Parks, M. M., Biggs, J., England, P., Mather, T. A., Nomikou, P., Palamartchouk, K., Papanikolaou, X., Paradissis, D., Parsons, B. and Pyle, D. M. (2012) 'Evolution of Santorini Volcano dominated by episodic and rapid fluxes of melt from depth', *Nature Geoscience*. Nature Publishing Group, 5(10), pp. 749–754.
- Pascal, K., Neuberg, J. and Rivalta, E. (2014) 'On precisely modelling surface deformation due to interacting magma chambers and dykes', *Geophysical Journal International*, pp. 253–278. doi: 10.1093/gji/ggt343.
- Phillipson, G., Sobradelo, R. and Gottsmann, J. (2013) 'Global volcanic unrest in the 21st century: An analysis of the first decade', *Journal of Volcanology and Geothermal Research*. The Authors, 264, pp. 183–196. doi: 10.1016/j.jvolgeores.2013.08.004.
- Pierson, T. C., Janda, R. J., Thouret, J.-C. and Borrero, C. A. (1990) 'Perturbation and melting of snow and ice by the 13 November 1985 eruption of Nevado del Ruiz, Colombia, and consequent mobilization, flow and deposition of lahars', *Journal of Volcanology and Geothermal Research*. Elsevier, 41(1–4), pp. 17–66.
- Pinel, V., Poland, M. P. and Hooper, A. (2014) 'Volcanology: Lessons learned from synthetic aperture radar imagery', *Journal of Volcanology and Geothermal Research*. Elsevier, 289, pp. 81–113.
- Poland, M., Hamburger, M. and Newman, A. (2006) 'The changing shapes of active volcanoes: History, evolution, and future challenges for volcano geodesy', *Journal of Volcanology and Geothermal Research*, 150, pp. 1–13. doi: 10.1016/j.jvolgeores.2005.11.005.
- Ranalli, G. (1995) *Rheology of the Earth*. Springer Science & Business Media.
- Rymer, H. and Tryggvason, E. (1993) 'Gravity and elevation changes at Askja, Iceland', *Bulletin of Volcanology*. Springer, 55(5), pp. 362–371.
- Rymer, H. and Williams-Jones, G. (2000) 'Gravity and Deformation Measurements', *Geophysical Research Letters*, 27(16), pp. 2389–2392.
- Satake, K. (2015) 'Geological and historical evidence of irregular recurrent earthquakes in Japan', *Philosophical Transactions of the Royal Society A: Mathematical, Physical and Engineering Sciences*, 373(2053). doi: 10.1098/rsta.2014.0375.
- Sella, G. F., Dixon, T. H. and Mao, A. (2002) 'REVEL: A model for Recent plate velocities from space geodesy', *Journal of Geophysical Research: Solid Earth*, 107(B4), p. ETG 11-1-ETG 11-30. doi: 10.1029/2000jb000033.

References

- Shibata, T., Suzuki, J., Yoshikawa, M., Kobayashi, T., Miki, D. and Takemura, K. (2013) 'Geochemical and Sr-Nd-Pb Isotopic Constraints on the Origin and Magmatic Evolution of Quaternary Lavas of Sakurajima Volcano, Southern Kyushu Island, Japan', *Bulletin of the Volcanological Society of Japan*, 58(1), pp. 43–58.
- Shichi, R. (2001) 'Gravity database of southwest Japan', *Bull. Nagoya University Museum, Special Rept.* the Gravity Research Group in Southwest Japan, 9.
- Singer, B. S., Le Mével, H., Licciardi, J. M., Córdova, L., Tikoff, B., Garibaldi, N., Andersen, N. L., Diefenbach, A. K. and Feigl, K. L. (2018) 'Geomorphic expression of rapid Holocene silicic magma reservoir growth beneath Laguna del Maule, Chile', *Science advances*. American Association for the Advancement of Science, 4(6), p. eaat1513.
- Smith, R., Sammonds, P. R. and Kilburn, C. R. J. (2009) 'Fracturing of volcanic systems: Experimental insights into pre-eruptive conditions', *Earth and Planetary Science Letters*. Elsevier, 280(1–4), pp. 211–219.
- Sparks, R. S. J., Biggs, J. and Neuberg, J. W. (2012) 'Monitoring volcanoes', *Science*. American Association for the Advancement of Science, 335(6074), pp. 1310–1311.
- Sparks, R. S. J. and Cashman, K. V. (2017) 'Dynamic magma systems: implications for forecasting volcanic activity', *Elements*. Mineralogical Association of Canada, 13(1), pp. 35–40.
- Svoboda, C., Rooney, T. O., Girard, G. and Deering, C. (2021) 'Transcrustal magmatic systems: evidence from andesites of the southern Taupo Volcanic Zone', *Journal of the Geological Society*. The Geological Society of London, (2), pp. jgs2020-204. doi: 10.1144/jgs2020-204.
- Tada, T. (1985) 'Spreading of the Okinawa Trough and its relation to the crustal deformation in the Kyushu (2)', *Zishin*, 38, pp. 1–12.
- Taira, A. (2001) 'Tectonic evolution of the Japanese island arc system', *Annual Reviews of Earth and Planetary Sciences*, 29, pp. 109–134.
- Tatsumi, Y., Otofujii, Y. I., Matsuda, T. and Nohda, S. (1989) 'Opening of the Sea of Japan back-arc basin by asthenospheric injection', *Tectonophysics*, 166(4), pp. 317–329. doi: 10.1016/0040-1951(89)90283-7.
- Taylor, N. C., Johnson, J. H. and Herd, R. A. (2021) 'Making the most of the Mogi model: Size matters', *Journal of Volcanology and Geothermal Research*. Elsevier, 419, p. 107380.
- Tiampo, K. F., Rundle, J. B., Fernandez, J. and Langbein, J. O. (2000) 'Spherical and ellipsoidal volcanic sources at Long Valley caldera, California, using a genetic algorithm inversion technique', *Journal of Volcanology and Geothermal Research*. Elsevier, 102(3–4), pp. 189–206.
- Todde, A., Cioni, R., Pistolesi, M., Geshi, N. and Bonadonna, C. (2017) 'The 1914 Taisho eruption of Sakurajima volcano: stratigraphy and dynamics of the largest explosive event in Japan during the twentieth century', *Bulletin of Volcanology*. Springer Verlag, 79(10). doi: 10.1007/s00445-017-1154-4.
- Tsutsui, T., Yagi, N., Iguchi, M., Tameguri, T., Mikada, H., Onishi, K., Miyamachi, H., Nishimura, T., Morita, Y. and Watanabe, A. (2013) 'Structure of Northeastern Sakurajima, South Kyushu, Japan, Revealed by Seismic Reflection Survey', *Bulletin of the Volcanological Society of Japan*, 58(1), pp. 239–250.
- UNISDR (2015) 'The human cost of natural disasters: A global perspective'. Centre for Research on the Epidemiology of Disaster (CRED).
- Uto, K., Miki, D., Uchiumi, S. and Ishihara, A. K. (1999) 'K-Ar dating and paleomagnetic measurements on drilled cores from the Sakurajima volcano: Preliminary attempts to reveal the history of the volcanic activity', *Kyoto Daigaku Bōsai Kenkyūjo nenpō*, (42), pp. 27–34.
- Wicks, C. W., Dzurisin, D., Ingebritsen, S., Thatcher, W., Lu, Z. and Iverson, J. (2001) 'Magmatic activity beneath the quiescent Three Sisters volcanic center, central Oregon Cascade Range, USA, inferred from satellite InSAR', in *AGU Fall Meeting Abstracts*, pp. G31C-0155.
- Wicks, C. W., Dzurisin, D., Ingebritsen, S., Thatcher, W., Lu, Z. and Iverson, J. (2002a) 'Magmatic activity beneath the quiescent Three Sisters volcanic center, central Oregon Cascade Range, USA', *Geophysical Research Letters*. Wiley Online Library, 29(7), pp. 21–26.
- Wicks, C. W., Dzurisin, D., Ingebritsen, S., Thatcher, W., Lu, Z. and Iverson, J. (2002b) 'Ongoing

References

- magma intrusion beneath the Three Sisters volcanic center, central Oregon Cascade Range, USA, inferred from satellite InSAR', in *Geological Society of America, Cordilleran Section, 98th annual meeting*, pp. 90–91.
- Williams, C. A. and Wadge, G. (1998) 'The effects of topography on magma chamber deformation models: Application to Mt. Etna and radar interferometry', *Geophysical Research Letters*. Wiley Online Library, 25(10), pp. 1549–1552.
- Williams, C. A. and Wadge, G. (2000) 'An accurate and efficient method for including the effects of topography in three-dimensional elastic models of ground deformation with applications to radar interferometry', *Journal of Geophysical Research: Solid Earth*. Wiley Online Library, 105(B4), pp. 8103–8120.
- Yamaguchi, K. (1975) 'Research on Sakurajima Volcano-Geological and Petrological Researches of the Surrounding Area of Kagoshima Bay and Sakurajima Volcano', *Educ. Soc. Earth Sci. Jpn.*
- Yamamoto, K., Sonoda, T., Takayama, T., Ichikawa, N., Ohkura, T., Yoshikawa, S., Inoue, H., Matsushima, T., Uchida, K. and Nakamoto, M. (2013) 'Vertical Ground Deformation Associated with the Volcanic Activity of Sakurajima Volcano, Japan during 1996 - 2010 as Revealed by Repeated Precise Leveling Surveys', *Bulletin of the Volcanological Society of Japan*, 58(1), pp. 137–151.
- Yamamoto, T., Takarada, S. and Suto, S. (1993) 'Pyroclastic flows from the 1991 eruption of Unzen volcano, Japan', *Bulletin of Volcanology*, 55(3), pp. 166–175. doi: 10.1007/BF00301514.
- Yang, X., Davis, P. M. and Dieterich, J. H. (1988) 'Deformation from inflation of a dipping finite prolate spheroid in an elastic half-space as a model for volcanic stressing', *Journal of Geophysical Research: Solid Earth*. Wiley Online Library, 93(B5), pp. 4249–4257.
- Yokoyama, I. (2013) 'Parasitic Eruptions on Sakurajima Volcano', *Bulletin of the Volcanological Society of Japan*, 58(1), pp. 91–102.
- Yokoyama, I. and Ohkawa, S. (1986) 'The Subsurface Structure of the Aira Caldera and its Vicinity in Southern Kyushu, Japan', *Journal of Volcanology and Geothermal Research*, 30, pp. 253–282.
- Zawalna-Geer, A., Hickey, J., Williamson, B., Petrone, C. M., Brown, J., Pickles, J. and Healey, J. (2019) '100 years of magma evolution at Sakurajima volcano, Japan', in *AGU Fall Meeting Abstracts*, pp. V13A-03.
- Zhang, Z. X. (2002) 'An empirical relation between mode I fracture toughness and the tensile strength of rock', *International journal of rock mechanics and mining sciences*. Pergamon, 39(3), pp. 401–406.
- Zienkiewicz, O. C. and Taylor, R. L. (2000) 'The Finite Element Method, Volume 1, The Basis', in *The Finite Element Method: Solid Mechanics*. Butterworth–Heinemann.